



저작자표시-비영리-변경금지 2.0 대한민국

이용자는 아래의 조건을 따르는 경우에 한하여 자유롭게

- 이 저작물을 복제, 배포, 전송, 전시, 공연 및 방송할 수 있습니다.

다음과 같은 조건을 따라야 합니다:



저작자표시. 귀하는 원저작자를 표시하여야 합니다.



비영리. 귀하는 이 저작물을 영리 목적으로 이용할 수 없습니다.



변경금지. 귀하는 이 저작물을 개작, 변형 또는 가공할 수 없습니다.

- 귀하는, 이 저작물의 재이용이나 배포의 경우, 이 저작물에 적용된 이용허락조건을 명확하게 나타내어야 합니다.
- 저작권자로부터 별도의 허가를 받으면 이러한 조건들은 적용되지 않습니다.

저작권법에 따른 이용자의 권리는 위의 내용에 의하여 영향을 받지 않습니다.

이것은 [이용허락규약\(Legal Code\)](#)을 이해하기 쉽게 요약한 것입니다.

[Disclaimer](#)

Master's Thesis

In-Process Laser Welding Monitoring by Fusing the
Uncertain Signal Information of Multi-Photodiode
Sensors

Rocku Oh

Department of System Design and Control Engineering

Graduate School of UNIST

2017

In-Process Laser Welding Monitoring by Fusing
the Uncertain Signal Information of Multi-
Photodiode Sensors

Rocku Oh

Department of System Design and Control Engineering

Graduate School of UNIST

In-Process Laser Welding Monitoring by Fusing the Uncertain Signal Information of Multi- Photodiode Sensors

A thesis
submitted to the Graduate School of UNIST
in partial fulfillment of the
requirements for the degree of
Master of Science

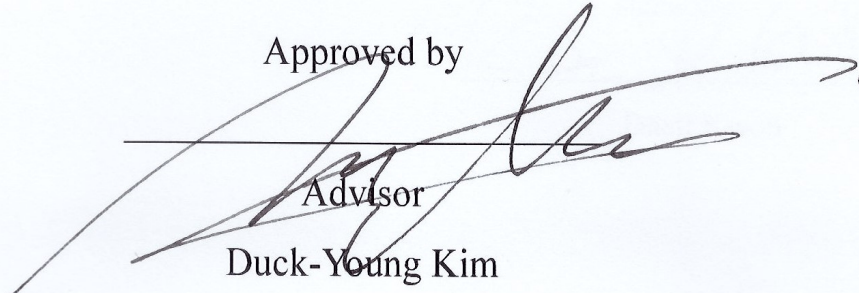
Rocku Oh

06. 29. 2017

Approved by

Advisor

Duck-Young Kim

A handwritten signature in black ink, appearing to read 'Duck-Young Kim', is written over a light blue rectangular background. The signature is fluid and cursive, with a long horizontal stroke extending to the right.

In-Process Laser Welding Monitoring by Fusing the Uncertain Signal Information of Multi- Photodiode Sensors

Rocku Oh

This certifies that the thesis of Rocku Oh is approved.

06. 29. 2017

signature

Advisor: Duck-Young Kim

signature

Hyungson Ki

signature

Daeil Kwon

Abstract

Remote laser welding is an emerging joining technology to meet the increasing demand of corrosion resistance, fast, non-contacted and single sided joining for automotive body-in-white assemblies. However, the quality of laser welding has been a critical issue in the popularization of this technology. Traditionally, various stochastic detection methods have been developed for in-process weld defect detection by monitoring and classifying various weld signals. The main objective of this thesis is to develop an in-process welding monitoring system including; (i) a novel defect detection algorithm based on a multi-sensor fusion technique, (ii) a new optical sensor configuration to capture in-process weld signal, and (iii) an offline weld signal analysis/training module and an user interactive online detection module.

The three weld signals are monitored: weld pool temperature, plasma intensity, and back reflected laser intensity. Their nominal trends are identified by estimating a probability distribution function for the signals and appropriate thresholds are specified by the standard statistical analysis of the residuals at the confidence interval of 95%. We propose a probability assignment function, characterized by shape controllability with respect to the extracted thresholds. We can analyze the in-tolerance defect problems by the proposed probability assignment function that can deal with the decision uncertainty near the thresholds. The individual sensor information is utilized to identify the probability of the normal state. The probabilities are aggregated by using the combination rule of the Dempster-Shafer theory. The performance of the developed detection method is evaluated by the statistical comparison with conventional visual inspection results.

Contents

I. Introduction.....	1
1.1 Background.....	1
1.2 Motivation	2
1.3 Objective.....	3
1.4 Outline of the thesis	4
II. Literature Survey.....	5
2.1 Process monitoring for laser welding	5
2.1.1 In-process monitoring.....	5
2.1.2 Post-process monitoring	10
2.2 Weld quality monitoring using sensor signals	12
2.2.1 Univariate approaches	13
2.2.2 Multi-sensor approaches.....	16
2.2.3 Uncertainty consideration.....	18
III. Laser Welding Quality.....	21
3.1 Mechanical Properties	21
3.2 Visual Inspection.....	22
3.2.1 Destructive test	22
3.2.2 Non-destructive test.....	22
3.3 The quality measure of laser welding	23
IV. Weld Defect Detection via Sensor Fusion under Uncertainty.....	25
4.1 Problem statement	25
4.2 Estimation of a probability distribution function for sensor data	28
4.3 Proposed probability assignment.....	29
4.3.1. The Dempster-Shafer theory.....	29
4.3.2. The thresholds adaptive probability assignment function	31
4.4 Multi-sensor evidence fusion by the Dempster's combination rule	37
4.5 Problem sets.....	41
4.5.1 Experimental setup	41
4.5.2 Experimental result and discussion	43
V. LaserWel: A Defect Detection and Monitoring System for Laser Welding	53
5.1 Optical system	54
5.2 Software development	58
VI. Conclusion and Future Research	63
References.....	65
Appendix.....	71
A. Experiments for the part-to-part gap size.....	71
B. Software registration	74

List of Figures

Figure 1-1 A variation of deformed base parts and angles of elevation and depression in a simplified side-member (Oh et al., 2016)	1
Figure 1-2 Part-to-part gap requirements with respect to the different base materials	2
Figure 1-3 A framework for the laser welding monitoring system	4
Figure 2-1 Acoustic sensor configuration (Shao and Yan, 2005).....	6
Figure 2-2 The spectral range of process signal in laser welding (Eriksson et al., 2010) and the dichromatic system for splitting the signal	7
Figure 2-3 Typical setups for optical detectors using co-axial and off-axial arrangements (Shao and Yan, 2005).....	7
Figure 2-4 Full and partial penetration during laser beam welding with ND-YAG lasers (Beersiek, 2001)	9
Figure 2-5 The keyhole images and their corresponding intensity profile (Bardin et al., 2005)	10
Figure 2-6 Trajectory of the vapor plume center relative to the keyhole position and exemplary images of the vapor plume recorded by camera (Brock et al., 2013).....	10
Figure 2-7 A Laser-Based Vision System for Weld Quality Inspection (Huang and Kovacevic, 2011).....	11
Figure 2-8 Typical X-ray image of seam welding (Kaftandjian et al., 2003)	11
Figure 2-9 Application of morphological filtering on radiographic binary images (Nacereddine et al., 2005)	12
Figure 2-10 Several univariate weld defect detection methods embedded in Precitec LWM™.....	13
Figure 2-11 Changes in the raw signals and the continuous RMS value (Lee et al., 2015).....	14
Figure 2-12 UV and IR Haar Wavelet signal and corresponding spectrogram for laser welding (Kim et al., 2013)	14
Figure 2-13 Electron temperature along the seam in which three holes have occurred. The peak points illustrated the place the holes appear (Rodill et al., 2010)	15
Figure 2-14 A result of experiment with metallic and sand inclusions - analysis with Cusum LS filter (Bebiano and Alfaro, 2009).....	15
Figure 2-15 A multivariate interpretation of two sensor data; datapoint(a) is classified as defect in terms of multivariate approach, and datapoint(b) is classified as normal even the value of sensor 2 exceeds the UCL	16
Figure 2-16 Process flow of the fuzzy pattern recognition system (Park et al., 2002)	18
Figure 3-1 A standard specification of the laser welding quality index	23
Figure 4-1 An illustration of conflict decision problem.....	25
Figure 4-2 An illustration of in-tolerance failure problem.....	26
Figure 4-3 An illustration of event pattern classification and the segmentation problem.....	27
Figure 4-4 A process flow of the general fault detection system	27
Figure 4-5 An example of PDF estimation result (Gamma distribution) of gathered temperature sensor data.....	28
Figure 4-6 The relation between Bel(A) and Pls(A).....	31
Figure 4-7 A best-fitted probability distribution function of plasma intensity signal	32
Figure 4-8 A comparison of proposed probability assignment function with respect to the magnitudeCoeff: (a) 1, (b) 3, (c) 5, (d) 20	33

Figure 4-9 An example of the adaptive probability assignment function of upper control limit: 23.4V, lower control limit: 11.7V, and midpoint:17.3V	33
Figure 4-10 A comparison of the adjusted probability assignment function with respect to the different weights(α): “ $\alpha=0$ ” implies that there is no further information of the estimated probability density function	34
Figure 4-11 A general guideline to define basic probability assignments of dual threshold interval(a) and modified probability assignment of $M(H, \neg H)$	35
Figure 4-12 A procedure of the defect detection system with the sensor fusion of each evidence	40
Figure 4-13 Experimental setup.....	42
Figure 4-14 Average probability of normal state and corresponding classification result of experiment #1	45
Figure 4-15 Average probability of normal state and corresponding classification result of experiment #2	45
Figure 4-16 Average probability of normal state and corresponding classification result of experiment #3	46
Figure 4-17 Average probability of normal state and corresponding classification result of experiment #4	46
Figure 4-18 A comparison of the F-scores corresponding the number of sources for sensor fusion	47
Figure 4-19 Mean voltage of reflection signal at each stitch	49
Figure 4-20 The F-scores with respect to the final decision threshold by changing the weight value(α)	50
Figure 4-21 The highest F-score with respect to the weights and the confidence intervals.....	50
Figure 5-1 A framework for the defect detection and process monitoring system.....	53
Figure 5-2 A prototype of the sensor system using Hamamatsu optics products.....	55
Figure 5-3 The schematic design of the photodiode sensor system for the process monitoring of laser welding.....	56
Figure 5-4 3D assembly design for the photodiode sensor system	56
Figure 5-5 A main panel of the developed monitoring software.....	59
Figure 5-6 An off-line training panel of the developed monitoring software	60
Figure 5-7 A reference selection panel for on-line monitoring of the developed monitoring software	60
Figure 5-8 Another version of developed monitoring software for production environment	61

List of Tables

Table 4-1 Dempster’s combination table for the two basic probability functions	37
Table 4-2 Boolean truth table for the combination of two basic probability function	38
Table 4-3 Chemical composition of experimental specimen (galvanized steel)	41
Table 4-4 Laser welding process parameter for the experiments	42
Table 4-5 The number of actual defected samples in the experiment #1 ~ #4	43
Table 4-6 Confusion matrix	44
Table 4-7 The performance metrics (precision, recall, and F-score) of the experiment #1	47
Table 4-8 The performance metrics (precision, recall, and F-score) of the experiment #2	47
Table 4-9 The performance metrics (precision, recall, and F-score) of the experiment #3	48
Table 4-10 The performance metrics (precision, recall, and F-score) of the experiment #4	48
Table 4-11 The highest F-scores of the sensitivity analysis with respect to the weights and the confidence intervals.	51
Table 5-1 Technical parameters of the laser source (IPG YLS-2000).....	54
Table 5-2 Technical parameters of the data acquisition system (NI cDAQ 9215)	55
Table 5-3 Detailed specifications of photodiode sensors	57
Table 5-4 Detailed specifications of filters for the sensors system	58

I. Introduction

1.1 Background

In the automotive industry, laser welding is an emerging joining technology that aims to meet the increasing demand for corrosion-resistant, lightweight and durable auto-body parts. The dynamic movement of the scanning head which adjusts the focal position of the laser beam without robot arm' maneuver, gives the laser welding process many advantages such as:

- ✓ Non-contact and single-sided access welding
- ✓ Fast and accurate welding
- ✓ Tool flexibility and less energy consumption as compared to conventional spot welding
- ✓ Reducing the required floorspace

Although laser welding with zinc coated steel has many of the advantages above, the requirement of tight part-to-part gap control, and thereby creating difficulties in weld quality control have been major barriers to the popularization of laser welding in automotive manufacturing due to the lower vaporization temperature point(1180K) than steel has 1809K. This tight part-to-part gap requirement is even more critical in the laser lap welding of galvanized steel since we should additionally ensure the minimum part-to-part gap between two steel sheets so that the vaporized zinc produced by the laser energy can be exhausted through the gap. As shown in Figure 1-1 and Figure 1-2, if the gap between the galvanized steel sheets is too small, it may cause weld defects such as porosity, spatter, an inter-metallic brittle phase or discontinuities formed by zinc vapor entrapment into the welding joints.

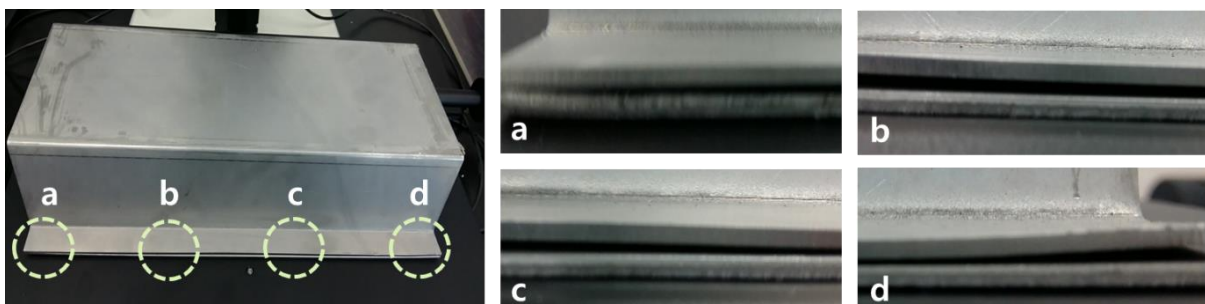


Figure 1-1 A variation of deformed base parts and angles of elevation and depression in a simplified side-member (Oh et al., 2016)

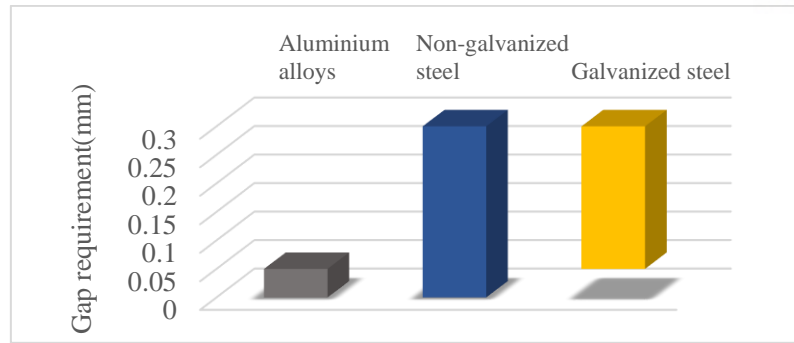


Figure 1-2 Part-to-part gap requirements with respect to the different base materials

1.2 Motivation

In addition to the tight requirement of the part-to-part gap condition, much of the empirical research has investigated the importance of the design parameters for laser welding. Some researchers have reported that several process parameters (the focal position, laser power, and feed rate) are significantly correlated with the weld quality: heat input and weld bead geometry (i.e., penetration depth, widths of welded zone, width of a weld seam, and heat-affected zone) (Benyounis and Olabi, 2008, Benyounis *et al.*, 2005). They have also validated several destructive tests which had been conducted after welding process in the real industry such as investigating a cross-sectional view and testing mechanical properties. General off-line destructive tests of weld quality, however, can be costly regarding time, material, and productivity.

To overcome this limitation of traditional off-line destructive tests, there has been a lot of research on on-line weld quality monitoring and defect detection by gathering and analyzing the process signals of the laser welding as an aspect of the non-destructive test. Various detection and diagnosis methods have been applied to online weld defect monitoring, for which the signals during the welding process should be monitored and classified quickly. Commercially available monitoring systems usually use univariate defect detection methods that require threshold values or reference curves which are determined by numerous pre-experiments to distinguish between normal and defect welds. A weld defect occurs if the sensor signal is out of the pre-defined permissible value and if the signal area exceeds the allowable tolerance. The on-line process monitoring approaches are beneficial for ensuring the high product quality at the high production rates and the low cost.

The real-time monitoring has utilized various sensors to promise the accuracy of defect detection. The commercially available laser welding monitoring systems usually use information from various

combinations of multiple sensors to increase the monitoring accuracy because no single sensor can reliably monitor the full spectrum of welding states. However, there are still some issues on the on-line monitoring systems. Integration of multiple sensors does not always guarantee the high accuracy of the detection performance. It creates the problem regarding the uncertainty of decision. We need to specify the causes of this uncertainty, especially on the commercially available monitoring systems. It is a main focal point of this research thesis.

First, a comprehensive decision and classification of the target state cannot be simply achieved by a multi-sensory monitoring system. There is a possible situation that the individual sensors indicated a different decision from the same state. Second, even if all the sensor signals are within the tolerance ranges, which implies that the interpretation of all sensors classifies the current state as normal, the actual defect might happen in a practical environment. This is called an in-tolerance failure problem. Third, specific signal patterns of weld defects may exist. It can be interpreted as a generalized version of the multiple thresholds problem. In this case, we need to choose the number of pieces of segments (binning problem), to codify the segmented pieces which is called codification (eventization) problem, and to interpret the series of codified segments which is related to the pattern recognition and process mining problem.

In this thesis, we focus on the first and the second issues by applying evidence theory and the proposed probability assignment function.

1.3 Objective

To enhance the accuracy of the defect detection performance, laser welding monitoring systems usually use rich information from multiple sensors such as plasma, temperature, and back reflection signals. However, interpreting multiple sensor information, each of which may indicate different weld quality status, is not straightforward as we discussed in the motivation section. In this regard, this research aims to first, develop a novel detection algorithm for weld defects based on multivariate information fusion technique. Also, we are further aiming to develop an in-process monitoring system including a new optical sensor configuration to capture in-process weld signal. Figure 1-3 illustrates the overall framework for a close-loop laser weld process monitoring and control, and which consists of two main phases: (i) the off-line analysis and training module for detection of weld defects and (ii) an in-process monitoring system for weld defect diagnosis. Further, we will consider the part-to-part gap assessment method which aims to realize the optimal process adjustment for the closed-loop process control.

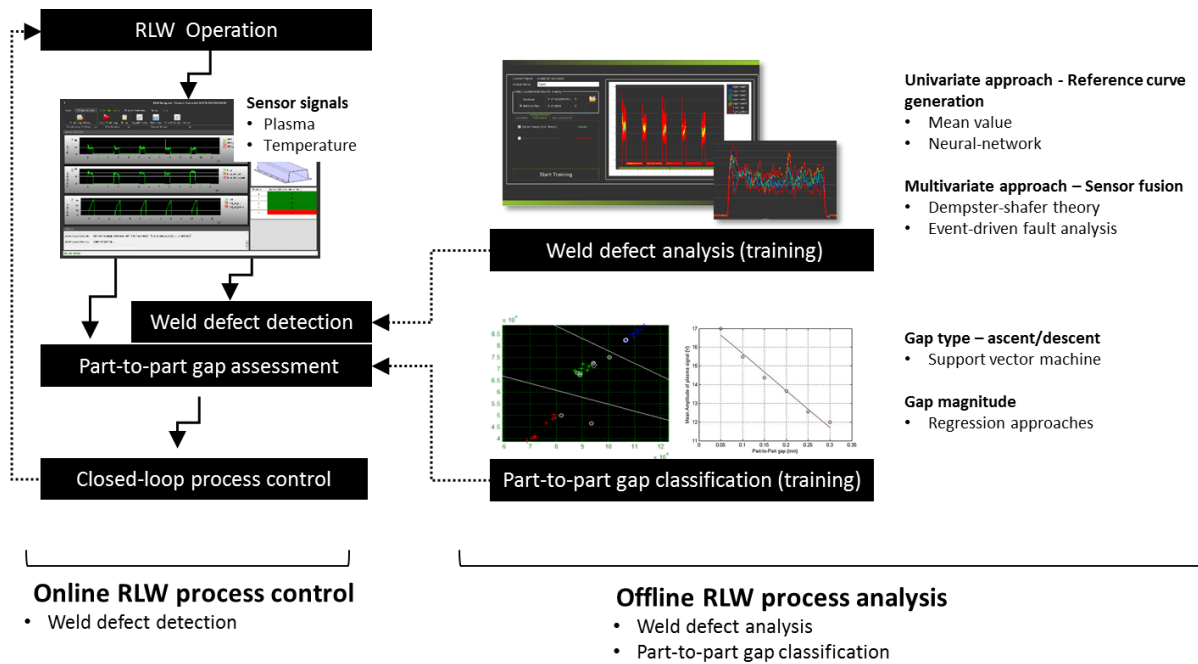


Figure 1-3 A framework for the laser welding monitoring system

1.4 Outline of the thesis

The paper consists of five chapters. The first chapter introduces the motivation and objectives of this paper. In Chapter 2, a literature survey on sensor system and data analysis for the monitoring of laser welding process are described. The quality measure of laser welding and relationship between the sensor signal and its weld quality for the paper are defined in chapter 3. In chapter 4, we define the problem that we focus on, and detailed procedures and methods for weld defect detection are described. A case study and the developed in-process monitoring system is described in Chapter 5. As a result, the conclusion and future research are described in Chapter 6.

II. Literature Survey

2.1 Process monitoring for laser welding

Several sampling tests such as mechanical test and visual inspection after welding process have been conducted to meet the demand for the quality level. Due to its characteristics of the non-contact and single-sided access, ensuring the quality of the joint assembly is one of the key issues on the realization of laser welding in an assembly line. Thus, complete quality inspection for every workpiece is needed to guarantee the quality of welded products. If proper and concise monitoring methods are adopted, the better productivity and the lower production cost can be achieved by reducing the number of production steps which is the sampling test and post-processing.

Over the past decade, number of research on monitoring the laser welding process have been conducted. The monitoring process is categorized by (i)when the monitoring procedure is conducted and (ii)which physical phenomenon is captured.

2.1.1 In-process monitoring

In-process monitoring is that process signals or images are gathered and analyzed during the joining process. It is also called as a real-time monitoring process. As the types of detectable emissions, we can categorize the monitoring system into three types, which are acoustic signal inspection, optical(light) signal inspection, and vision inspection. Each process signal contains different information on laser-material interaction, which can monitor and detect weld defects during the welding process for every workpiece. Thus, proper sensors should be used to measure those emissions of the welding process.

Shao and Yan(Shao and Yan, 2005) reviewed the techniques for on-line monitoring and inspection of laser welding. They investigated various types of the signal such as acoustic emission, light emission, the intensity of plasma emitted from the welding area and reflected light in order to monitor the process condition.

Acoustic signal inspection

Acoustic emissions are induced by changing the internal structures, metal vapor the surface and reflected laser beam from the welded parts. Those signals can be gathered a sensor which can convert acoustic waves into an electrical signal(e.g. voltage, ampere). A microphone placed nearby weld zone, which is generally used to collect the signals, was used to collect a signal of wavelength ranges between 20Hz and 20kHz. The frequency band contains a sort of diagnostic information on weldment morphology, penetration depth, and the heat-affected zone. A study on the range conducted by Gu and Duley(Gu and Duley, 1996) developed discriminant function using these spectral components for classification on laser weld into three different classes: overheated, full penetration and non-penetration or partial penetration. More detailed monitoring of the welding process was achieved through analyzing the time-frequency properties of the acoustic emission signals than can be obtained through the statistical analysis and simple magnitude measurements. Zeng et al. (Zeng *et al.*, 2001) defined signal intensity moving average(IMA) curve via wavelet analysis, and the curve effectively recognized the transitions of welding states and identifying defects.

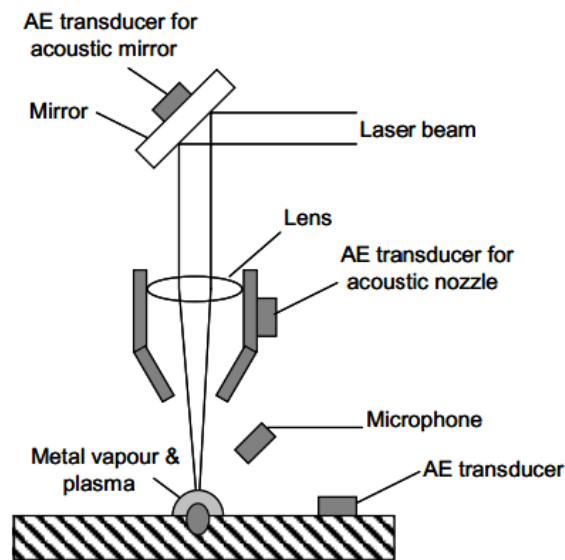


Figure 2-1 Acoustic sensor configuration (Shao and Yan, 2005)

Higher frequency band over 50kHz is usually gathered by piezoelectric transducers mounted on workpieces. Li installed ultrasonic piezoelectric sensors on the beam mirrors. Welding process conditions varied to verify the response of various acoustic sensors with respect to the heating, melting, vaporization, plasma generation and keyhole generation(Li, 2002).

Due to its low cost for installation and relevance on machining characteristic, the acoustic signal was easily applied to monitor and analyze the welding process. Although those benefit above, the

limitation of acoustic signal monitoring in harsh environments is evident. The acoustic signal monitoring system usually has been hard to implement at the industrial site because of high noise level from surroundings (Park, 2012). It has to be contacted with the weld pieces and exposed to high temperatures, and it makes piezoelectric sensors be impractical in industrial level also.

Radiation(light) signal inspection

Photodiodes and spectrosopes are widely used to convert the radiation emission (typically ultraviolet(UV) and infrared(IR) ranges) during the laser welding process into an electrical signal. Usually, the sensors are installed at the co-axial direction of the laser beam with several filters to confine the wavelength ranges of the each sensor. The combination of different photodiodes helped to carry out independent detection of plasma radiation, laser reflection, and thermal emission (Olsson *et al.*, 2011).

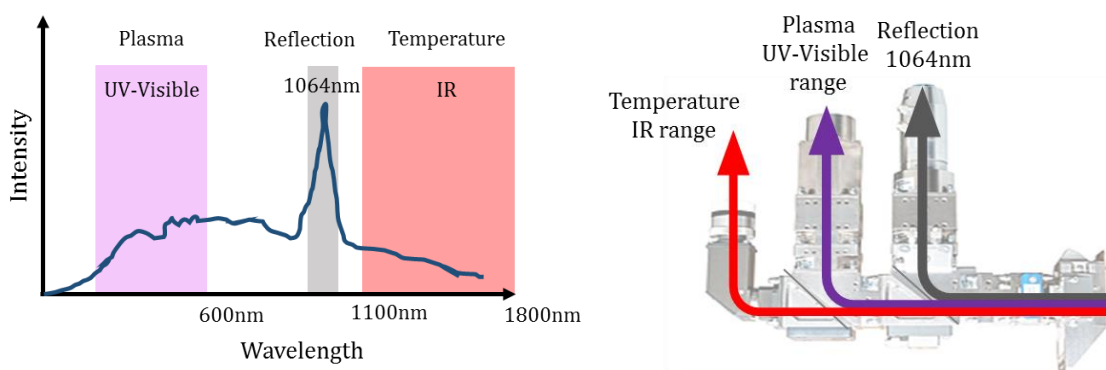


Figure 2-2 The spectral range of process signal in laser welding (Eriksson *et al.*, 2010) and the dichromatic system for splitting the signal

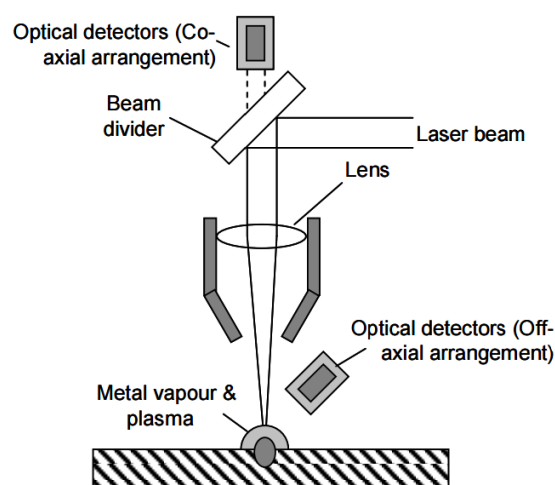


Figure 2-3 Typical setups for optical detectors using co-axial and off-axial arrangements (Shao and Yan, 2005)

Ultraviolet(UV) range

For laser welding, the generated plasma is known to emit light with a wavelength between 190nm and beyond 400nm (Park *et al.*, 2002). This spectral range is directly related to the state of plasma plume. Detailed information on keyhole oscillation and penetration depths can be achieved by analyzing the signal spectrum.

Sibillano *et al.*(Sibillano *et al.*, 2005) investigated the dynamics of the plasma plume through an optical spectroscopic approach. They performed a correlation analysis of the optical spectrum using covariance mapping technique. Tu *et al.*(Tu *et al.*, 2002) quantitatively characterized the plasma absorption of a laser beam inside the keyhole.

Zhang *et al.*(Zhang *et al.*, 2005) insisted that keyhole plasma has effects on energy transfer efficiency to the material, a variation of molten pool width, and penetration depth. Bardin *et al.*(Bardin *et al.*, 2005) also concluded the UV frequency range of the signal clearly indicated the presence of a fully opened keyhole, thus ensuring a fully penetrated weld.

IR range

The infrared signal, which is in the wavelength range of 1100~1700 nm typically, is related to the information on weld pool temperature and heat affected zone(You *et al.*, 2014). The signal inferred width of the surface bead and occurrence of spatters which emits light with a wavelength between 1000nm and 1600nm.

Park *et al.*(Park and Rhee, 1999, Park *et al.*, 2002) monitored the bead shape by a photodiode-based acquisition system for the infrared emission from weld pool and spatters. A measurement of the spectral intensity of the IR radiation from the weld pool gave information on the weld pool temperature and occurrence of irregular shape.

Colombo and Previtali(Colombo and Previtali, 2009) have investigated the on-line monitoring of fiber laser welding performed on Titanium alloy. The author concluded that the time domain features of infrared waveband (1150–1800 nm) intensity reflected welding defects such as power decreases, shielding gas flow rate decrease, and lack of penetration.

Jeon *et al.*(Jeon *et al.*, 1998) analyzed transient heat flow of the surface temperature based on the finite element method using an infrared radiation sensor.

Reflected laser light range

In addition, the reflected laser is also gathered to specify the amount of the radiation of the laser source which is not absorbed by the material. The signal range is slightly different with respect to the laser sources; fiber laser(1064nm) and disc laser(1030nm)(Kim *et al.*, 2008).

Many types of research have proved that the amount of laser reflection is sensitive to the variation of keyhole size(ISO, 1996). A larger amount of reflected signal were detected as the keyhole expands, while the less reflected if the keyhole was shrunk(ISO, 2001).

Vision inspection

On-line vision sensor such as CCD/CMOS and IR camera are widely used to monitor the current status of the laser welding process. Unlike the acoustic and photodiode sensors, vision system, which can capture the still images, can directly cater of information on monitoring status and further weld defects.

Beersiek(Beersiek, 2001, Beersiek, 1999) presented a coaxial CMOS-based monitoring system for laser beam welding. The system observed the geometrical parameters of keyhole formation. Zhang et al. (Zhang *et al.*, 1996) also measured the geometrical appearance of the weld pool using the vision camera system. Additionally, they utilized the neural network algorithm to identify the parameters in real time.

Brook et al.(Brock *et al.*, 2013) utilized two high-speed cameras to capture the synchronous vapor images. The observation direction of camera-1 and camera-2 was installed at 90° angles each with a frame rate of 6000 fps and an exposure time of 2μs. They observed fluctuations of 3D vapor plume during overlap welding of steel sheets. Based on the plume position, they analyzed relevant information on the process state.

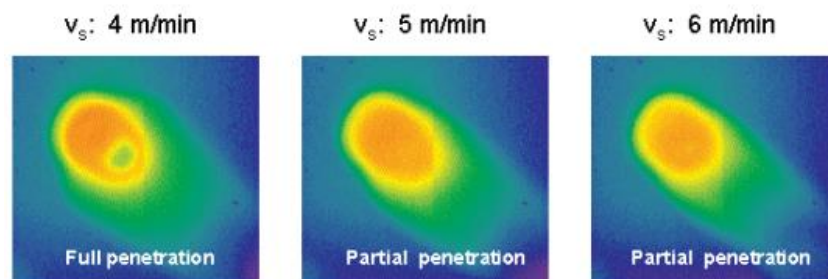


Figure 2-4 Full and partial penetration during laser beam welding with ND-YAG lasers (Beersiek, 2001)

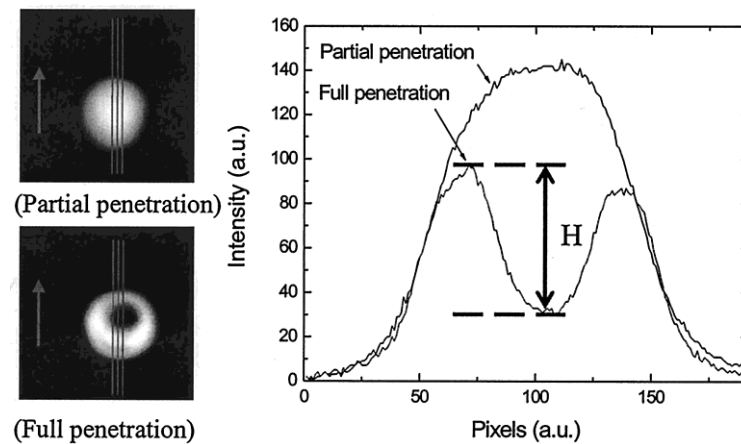


Figure 2-5 The keyhole images and their corresponding intensity profile (Bardin et al., 2005)

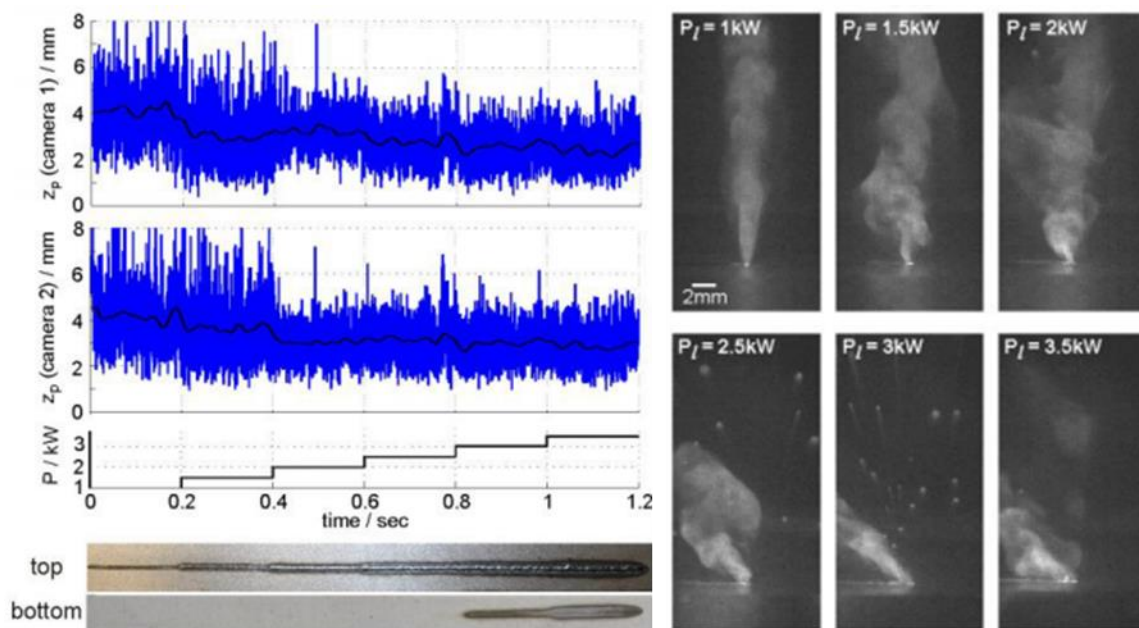


Figure 2-6 Trajectory of the vapor plume center relative to the keyhole position and exemplary images of the vapor plume recorded by camera (Brock et al., 2013)

2.1.2 Post-process monitoring

The purpose of the post-processing stage is not only to identify and detect the weld defects automatically but to visualize the better image information for supporting the decision of human inspectors. Usually, the vision based inspection was used to monitor the process status and weld quality right after the

completion of the welding process.

Luo and Chen (Luo and Chen, 2005) used a Meta 3D camera and a Keyence position-sensitive-detector (PSD) laser displacement sensor to be capable of tracking V-groove, fillet, lap and butt joints of welding with the high accuracy of less than 0.4 mm error.

Huang and Kovacevic (Huang and Kovacevic, 2011, Huang and Kovacevic, 2012) developed a similar laser-based vision system for non-destructive weld quality inspection. They used point laser generator and the image receiver for capturing the geometry of weld seam and further surface weld defects. The point laser was projected onto the surface. The scattered and reflected laser light were detected by the image sensor. The vision sensor was designed based on the principle of laser triangulation.

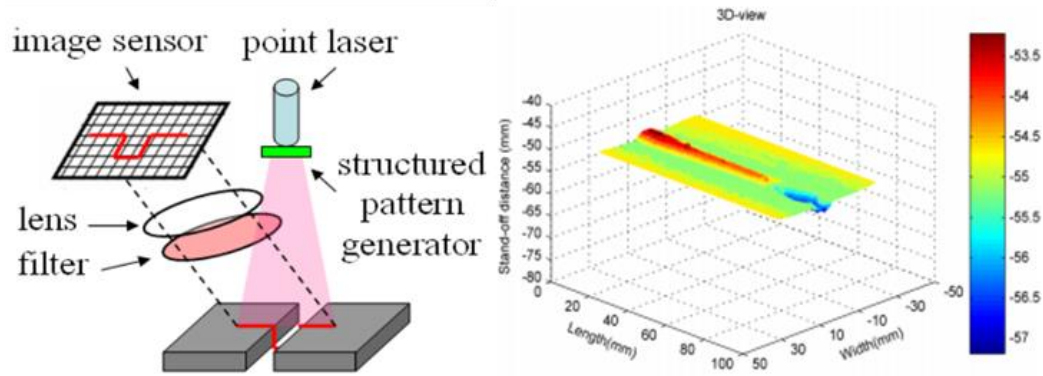


Figure 2-7 A Laser-Based Vision System for Weld Quality Inspection (Huang and Kovacevic, 2011)

Other inspection systems and techniques have been investigated by many researchers. Kaftandjian et al. (Kaftandjian *et al.*, 2003) used the x-ray images and proposed a fuzzy based algorithm to detect weld defects. Nacereddine et al. (Nacereddine *et al.*, 2005) also presented industrial radiography approach to investigate internal defects.

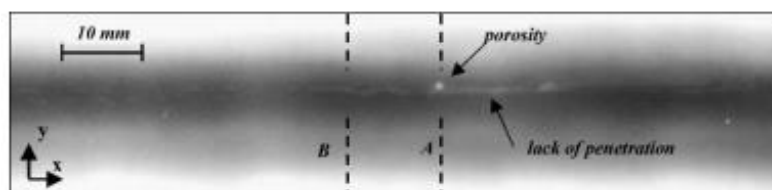


Figure 2-8 Typical X-ray image of seam welding (Kaftandjian et al., 2003)

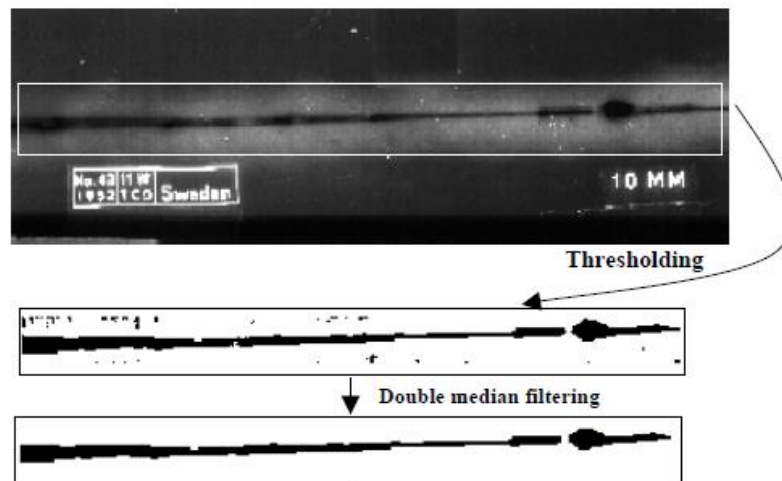


Figure 2-9 Application of morphological filtering on radiographic binary images (Nacereddine et al., 2005)

Another approach (Kaftandjian *et al.*, 2003) is to utilize ultrasound-based inspection system for weld quality by monitoring the weld pool. The ultrasound generated by the laser phased array propagated through the weld pool and was gathered by the non-contact electromagnetic acoustic transducer (EMAT) receiver.

2.2 Weld quality monitoring using sensor signals

As the use of monitoring system for laser welding process has increased, so does the need for reliable defect detection methods for process monitoring. Several experimental approaches have been undertaken to resolve the accuracy problem. Single sensor approach is relatively easy and fast way to detect defects. However, if only the use of the IR range of photodiode, defects caused by fluctuation of plasma plume cannot be detected. No single sensor, thus, can reliably monitor all laser welding processes. For that reason, two main solutions or stream arose to overcome the drawback. The first is to install a series of same sensors to increase signal reliability, and the other is to use heterogeneous sensors to get different physical responses.

2.2.1 Univariate approaches

Commercially available monitoring systems usually used univariate defect detection methods that require threshold values or reference curves to distinguish between normal and defective status. In general, those thresholds are determined by numerous pre-experiments that are costly and time-consuming. As shown in Figure 2-10, it is possible to consider that weld defect occurs if the sensor signal moves out of the pre-defined allowable value, and/or if the signal area exceeds the allowable tolerance. Note that the signal area calculation starts when the signal is outside the tolerance band and ends when the signal moves into the tolerance band again.

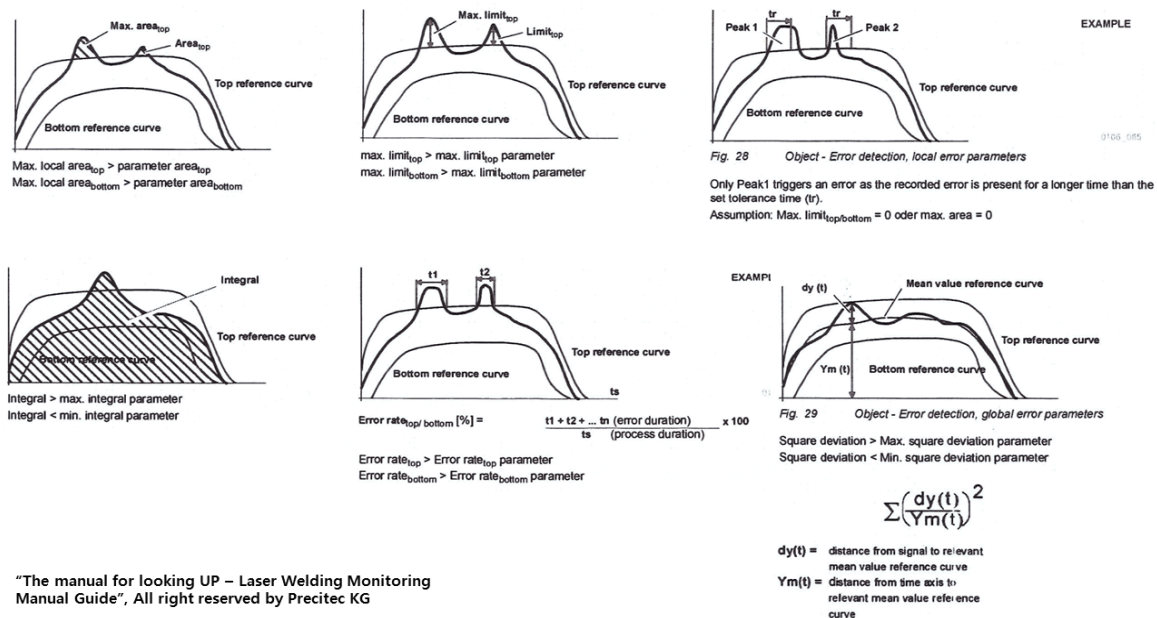


Figure 2-10 Several univariate weld defect detection methods embedded in Precitec LWM™

Lee et.al (Lee *et al.*, 2015, Kim and Lee, 2010) analyzed the RMS value of acoustic emission as well as light(plasma) emission as a function of lap clearances with Zn coated thickness. The results indicated that RMS values increased depending on the amount of Zn vaporization, and RMS also changed abruptly when defects occurred depending on lap joint conditions They found that when the frequency value was set to the bandwidth of bandpass filter, the filtered RMS values matched to the corresponding weld defects. Thus they have considered that the filtered RMS signals and defects were very closely related to the defects.

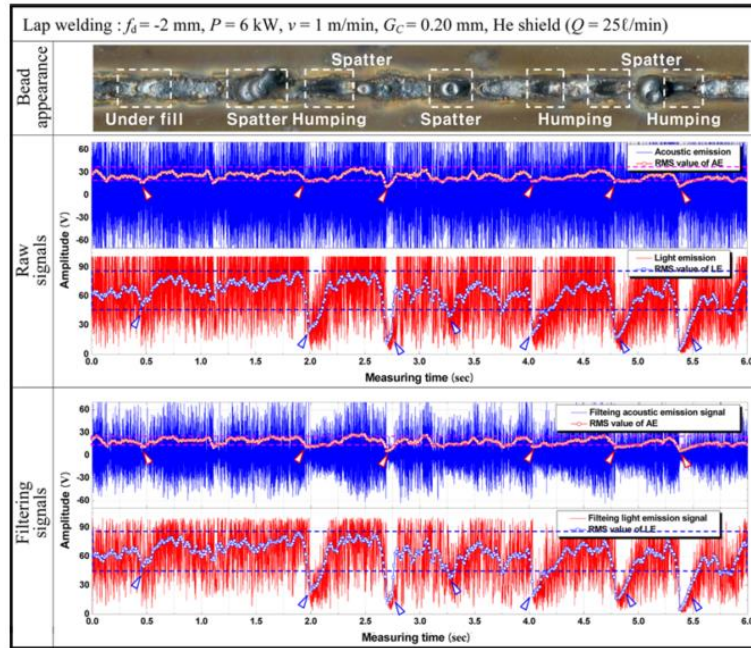


Figure 2-11 Changes in the raw signals and the continuous RMS value (Lee et al., 2015)

Kim et.al(Kim *et al.*, 2013) investigated that the correlation between the plasma electron temperature and the presence of weld defects. They decomposed the radiation signal into UV and IR ranges captured during the welding. Each signal was converted to wavelet filtered signal using Harr wavelet. The generated signals were converted to the spectrogram. They detected weld defect if the transformed signal was inside of the pre-defined threshold boundary.

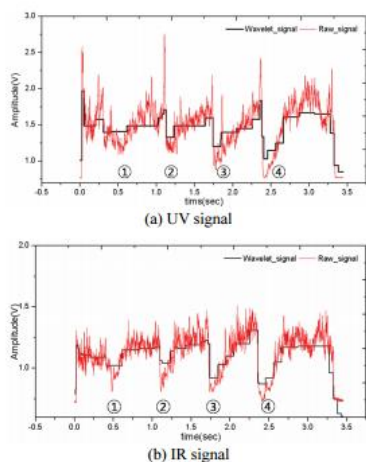


Fig. 14 UV and IR Haar Wavelet signal for laser welding

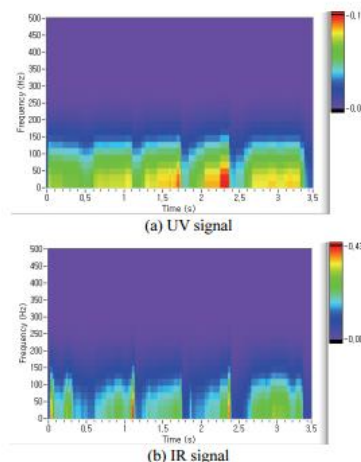


Fig. 15 UV and IR Spectrogram of Wavelet signal for laser welding

Figure 2-12 UV and IR Haar Wavelet signal and corresponding spectrogram for laser welding (Kim et al., 2013)

Rodill et al.(Saludes Rodil *et al.*, 2010) calculated electron temperature and compared with defect occurrences. The proper settings of the threshold effectively detected the weld defect. The problem was to find threshold and parameter settings and to determine which of the abrupt changes in the signal were associated.

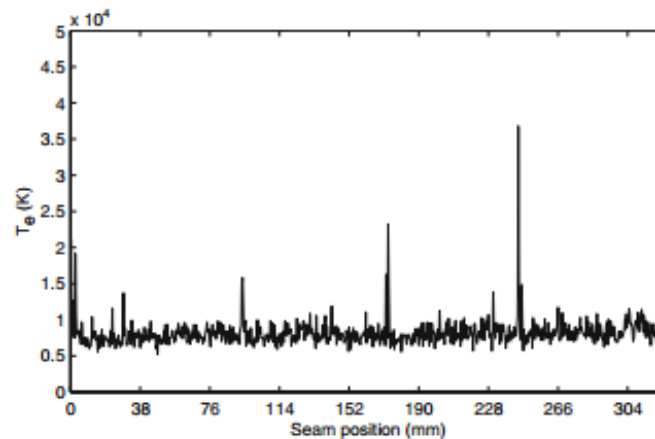


Figure 2-13 Electron temperature along the seam in which three holes have occurred. The peak points illustrated the place the holes appear (Rodill et al., 2010)

Bebiano and Alfaro(Bebiano and Alfaro, 2009) proposed advanced change detection algorithm, which was CUSUM LS filter algorithm, to detect defects caused by metallic inclusions, gas disturbance and sprayed water. The main advantage was that there was no need in calculating the electron temperature which was hard to calculate exactly.

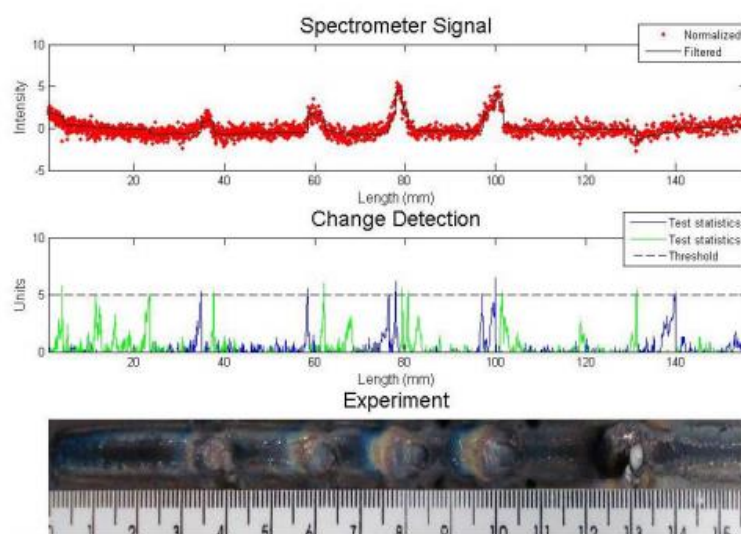


Figure 2-14 A result of experiment with metallic and sand inclusions - analysis with Cusum LS filter (Bebiano and Alfaro, 2009)

Zeng et al.(Zeng *et al.*, 2001) defined signal intensity moving average(IMA) curve via wavelet analysis, and the curve effectively recognized the transitions of welding states and identifying defects.

Luo et al.(Luo *et al.*, 2005) used back-propagation (BP) neural network with three layers to diagnose welding defects such as gap and misalignment using the audible sound from the laser-induced plasma plume during keyhole laser welding. They decomposed the acoustic signal into a series of approximations and details distributed over different frequency bands. The decomposed levels were used for input variables for the neural network.

Eriksson and Kaplan (Eriksson and Kaplan, 2009) studied a commercial system with three detectors for nine different industrial welding applications. Weld defects were analyzed and explained by the each signal. They found that the temperature and the plasma sensor had a high correlation to the fluctuation of the observed plume above the keyhole. Humping defect was observed by the temperature sensor whereas the rapid events of blowouts were concealed by the fluctuations of the plume. They concluded that understanding of the signal source facilitated the reliable application of monitoring systems.

2.2.2 Multi-sensor approaches

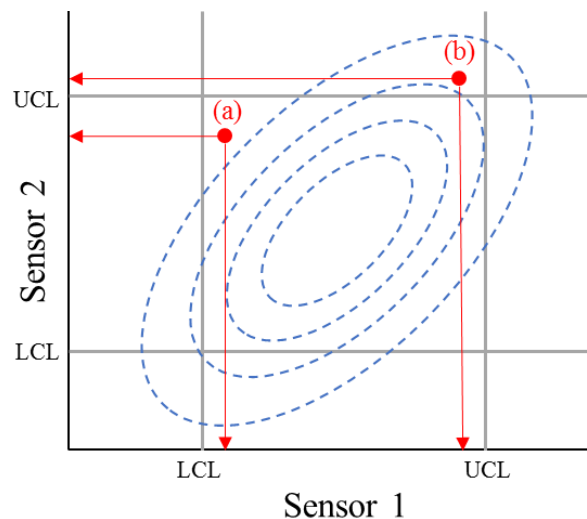


Figure 2-15 A multivariate interpretation of two sensor data; datapoint(a) is classified as defect in terms of multivariate approach, and datapoint(b) is classified as normal even the value of sensor 2 exceeds the UCL

As shown in Figure 2-15, univariate defect detection methods cannot sufficiently explain and reflect multi-sensory system and its characteristics. Generally, a laser welding monitoring systems use rich information from multiple sensors such as multiple combinations of radiation emission photodiodes and vision sensors simultaneously, which are used for detecting defective status. Two main solutions or stream arose to capture the rich information. The first is to install a series of same sensors to increase signal reliability. The second is to use heterogeneous sensors to get different physical responses. Multivariate approaches which can interpret inter-information between sensors are needed to make up for the drawback of univariate fault detection to enhance the accuracy and reliability of defect detection system.

Colombo et al.(Colombo *et al.*, 2013) compared different methods to monitor and analyze the visible emission. They evaluated the monitoring methods to identify the effects of variable factors, such as the gap between the plates and the location of the weld seam at which the variation of the gap occurs, on the monitored emission. Multivariate data analysis was used to evaluate different indicators, variance analysis is performed, and the statistical significance of the gap value and its location in the weld seam were used to compare the performance of the tested methods.

Li et al.(Li *et al.*, 2010) have researched on the weld bead vision measurement and the defect detection by the light-based vision inspection system. They developed an inspection system which can monitor weld bead dimensions to detect defects based on the measurements of groove width, weld bead width, filling depth, reinforcement height, plate displacement, weld bead misalignment, and undercut.

Eriksson et al.(Eriksson *et al.*, 2010) investigated on the independent information about the thermal condition of the melt (the T signal), the radiation from the plume of a heated gas above the melt (the P signal) and the amount of reflected laser light (the R signal). They suggested that the correlation between the temperature and plasma signals is so strong that a temperature–plasma signal would be more useful than the raw T signal in identifying the fluctuations of the infrared radiation from the melt pool.

Zhang et al.(Zhang *et al.*, 2008) estimated the welding penetration state by monitoring the infrared, ultraviolet and sound emission. They utilized the neural network algorithm as an information fuser for estimating the weld penetration. The PSO-BP algorithm was applied to increase the learning speed of the coefficients.

Sun et al.(Sun *et al.*, 2002) have evaluated the feasibility of real-time nondestructive weld penetration detection using sensor fusion of IR, ultraviolet (UV), audible sound (AS), and acoustic emission (AE) sensors.

You et al.(You *et al.*, 2014) reviewed the multi-sensor fusion technologies of both laser welding

monitoring and adaptive control. They insisted that the online defect detection and monitoring technologies were far from perfect, and the detection accuracy for different welding statuses and defects was expected to be improved. Moreover, as an aspect of the hardware system for the monitoring such as sampling frequency and resolution, the computing speed of intelligent signal processing and recognition technology were also restricted. Also, little research has been conducted on adaptive control during the welding process, and the controlled variables were mainly confined to the low-power laser system.

2.2.3 Uncertainty consideration

Park et al.(Park *et al.*, 2002) developed a real-time evaluation system for the quality of the laser welding. They measured the plasma and spatters generated during laser welding are measured using two UV and an IR photodiode. To perform real-time evaluations of the weld quality, the system used a fuzzy multi-feature pattern recognition using the measured signals. The process flow of the system is illustrated in Figure 2-16. Kuhl et al.(Kuhl and Neugebauer, 2006) also developed a fuzzy pattern technique where the entire welding seam was tested for faults by visual inspection and radioscopy as reference techniques. The method resulted in improved prediction of seam irregularities comparing with the conventional methods.

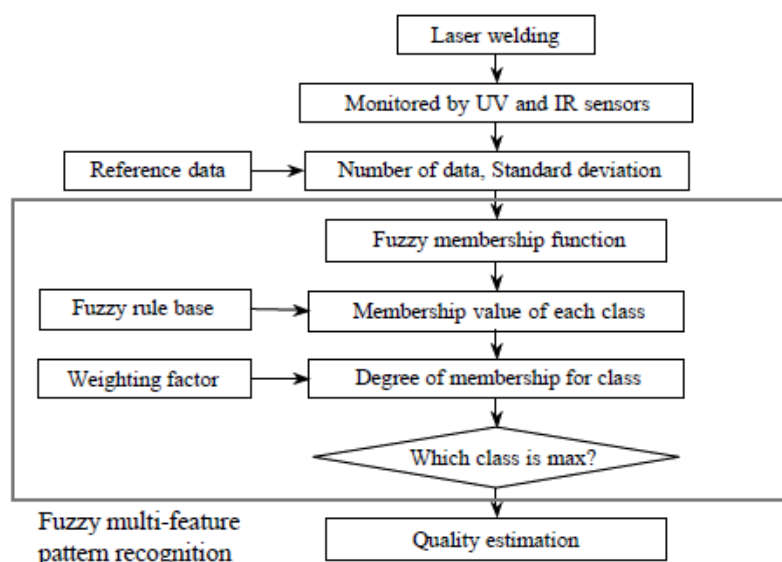


Figure 2-16 Process flow of the fuzzy pattern recognition system (Park et al., 2002)

Basir and Yuan(Basir and Yuan, 2007) investigated the use of Dempster–Shafer evidence theory

as a tool for modeling and fusing multi-sensory evidence in fault diagnosis of an automotive engine. They introduced two new methods for enhancing the effectiveness of mass functions in modeling and combining the evidence. They presented a criterion to evaluate the performance of the proposed information fusion system also.

Kaftandjian et al.(Kaftandjian *et al.*, 2003) presented an approach based on the combination of Dempster–Shafer theory and fuzzy sets for improving detection of weld defects. They modeled the uncertainty in detecting defects from the visualized weld images. The results obtained in the case of X-ray weld inspection have shown that up to 80% of defects with a credibility of about 0.55 have been detected without any false alarm.

This Page Intentionally Left Blank

III. Laser Welding Quality

The way of measuring the weld quality is categorized based on two properties. The mechanical properties is a conventional testing method for measuring the joint quality. By testing the strength of the joint material, one can compare that the current weld joint quality is good or bad. Traditionally, tensile strength, which is one of the test joint strengths of the industrial standards, is measured by the maximum stress that a material can withstand while being stretched or pulled before breaking. Additionally, several visual inspection tests of joint parts have been conducted.

3.1 Mechanical Properties

Mechanical properties of welds such as hardness, fatigue, tensile strength, and other important structural properties were discussed.

Ma et al.(Ma *et al.*, 2014) investigated the tensile strength of the hardened zone (fusion zone and the grain coarsened heat affected zone (HAZ)), the softened zone (subcritical HAZ), and the base material under the condition of high strength dual phase (DP) 980 steel lap joint. They compared the experimental result of the numerical prediction of von Mises equivalent strain concentrations with failure modes, and the comparison exhibits reasonable agreements.

Chen et al.(Chen *et al.*, 2009) evaluated the welding of the lap-joint configuration of hot-dip galvanized steel sheets through an optical scanning and electron microscopy with the tensile/hardness tests. They drilled holes between two sheets to vent zinc vapor effectively. They found that the small increase of hardness in “joint gap” and “vent hole” approaches because of the absence of gas porosity. The vent holes method led welds to be stronger, more aesthetic, and porosity-free compared to the existing “joint gap” method. The welds produced by using “vent holes” configuration also have higher tensile strength than the regular configuration of joint gap.

Mei et al.(Mei *et al.*, 2013) compared two types of laser system as a hardness and tensile strength as well as surface formation and cross-sectional weld shape. The hardness of fiber laser welding joint (weld zone and heat-affected zone) is slightly higher than that of CO₂ laser welding joint without exception. With the appropriate technological parameters, the tensile-shear capacity is also better when using the fiber laser compared with CO₂ laser welding test pieces.

Mei et al.(Mei *et al.*, 2009) studied the effects of process parameters such as laser power, welding

speed, focal position, shielding gas and zinc vaporization on the mechanical weld quality. The experimental results indicated that both the tensile strength and microhardness of welding joints were higher than those of the base metal under the chosen conditions.

3.2 Visual Inspection

The difference of visual inspections compared to the testing the mechanical properties is the way of non-destructive tests. The mechanical testing should be followed by the welding process, and thereby producing another processing step of the production line. The advantage of the non-destructive test is to reduce at least one production step, and thus reducing production time and its corresponding cost.

3.2.1 Destructive test

The visual inspection can be conducted by destructing the test weld specimen. A cross-sectional view provides the visual shape of the weld joint part. From the shape, one can detect weld defects inside of the weld bead such as crack, porosity, and depth of penetration. Generally, the weld cross-section formed the shape of “Y” (wide at the top and narrow at the bottom) if the CO₂ laser is utilized for welding. The cross-sectional shape is similar to “I” with almost the same upper and lower part width when using fiber laser (Mei *et al.*, 2013).

3.2.2 Non-destructive test

Westerbaan *et al.* (Westerbaan *et al.*, 2014) investigated the influence of the amount of concavity on the tensile and fatigue properties of the welds in the condition of fiber laser welds. The amount of concavity was measured by taking the ratio of the reduction in area from the sheet thickness in the fusion zone (FZ) to the initial sheet thickness. They concluded that large concavity of 25 to 35% reduced the tensile strength of the DP980 welds.

The relationship between non-destructive testing and the corresponding mechanical properties should be considered. Investigation of seam width, length, and its variation was somewhat related to the tensile strengths. Sinha *et al.* (Sinha *et al.*, 2013) have concluded that relationship between the variation of weld seam and tensile shear strengths were correlated in the laser welding of galvanized steel in a lap joint configuration. They insisted that the variation of weld seam could be one of the

potential joining quality estimators. From the research, the variation of weld seam could be used as an indirect measure for estimating the tensile strength.

Further, Eriksson and Kaplan(Eriksson and Kaplan, 2009) investigated the comparison of the surface defect and its radiation signal. Humping can be observed by the temperature range of the photodiode sensor. A reflected laser light also can be useful to judge the quality of the weld.

3.3 The quality measure of laser welding

Based on the previous studies and researches, a non-destructive test of visual inspection sufficiently is the indirect measure of mechanical properties. The visual inspection(weld quality) standard differs from the need of industrial level and companies.

In this paper, we utilized modified version of the laser welding quality index from of an industrial standard specification as shown in Figure 3-1. If either partial penetration(lack of penetration), spatter, penetration hole, or porosity occurs on a stitch, the stitch is classified as a bad-welded(defect) stitch.

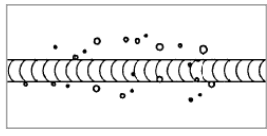
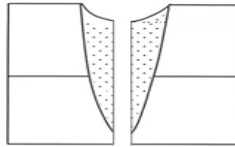
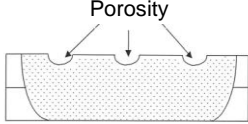
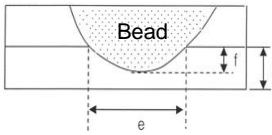
	Criteria	criteria
Spatter		No spatter on welding bead
Penetration hole		No penetration hole on welding bead
Porosity		No porosity on weld bead ※ undercut along a direction of weld bead
Partial penetration		100% full penetration needed (back bead) ※ In case of outer hemming parts for good appearance, larger than 10% partial penetration

Figure 3-1 A standard specification of the laser welding quality index

This Page Intentionally Left Blank

IV. Weld Defect Detection via Sensor Fusion under Uncertainty

4.1 Problem statement

To enhance the accuracy of the defect detection performance, laser welding monitoring systems usually use rich information from multiple sensors such as plasma, temperature, and back reflection signals. However, it is not straightforward to interpret multiple sensor information as we discussed in Chapter 1. It ultimately arises the problem regarding uncertainty in defect detection. We need to specify the causes of the uncertainty, in particular on the commercially available monitoring system. It is the focus point of the thesis.

First, the final decision or classification of the target state cannot be simply achieved by the monitoring system consists of multiple sensors, each of which may indicate different weld quality status. It means that the individual sensors decide different decision simultaneously as shown in Figure 4-1. For example, plasma detector classifies that current welding state is defective, whereas temperature detector decided as a normal state.

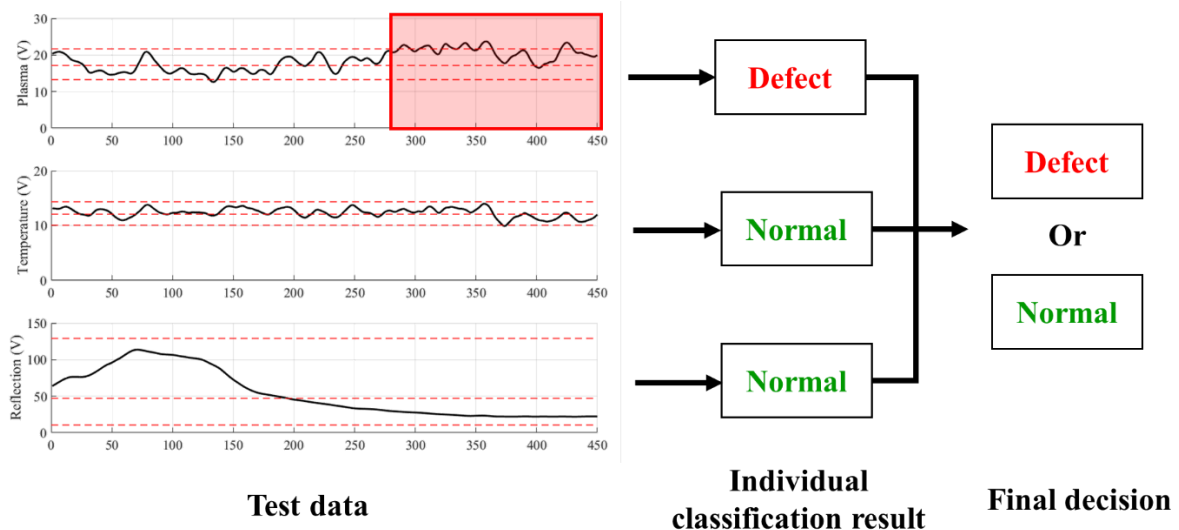


Figure 4-1 An illustration of conflict decision problem

Second, even all the sensor signals are within the tolerance range, and thus, interpretation of each decision of the sensors are straightforward to classify or decide it as the same result, the actual defect may have happened in a practical environment. It is called in-tolerance failure problem. The single hyperplane or threshold is not sufficient to reflect this type of problem in this case. We should consider each signal carefully as shown in this Figure 4-2. The temperature signal has bounded the bottom threshold, which means that all the data points of the temperature sensor are inside of the thresholds. The trend and signal level, however, is highly close to the threshold, which may cause the defects.

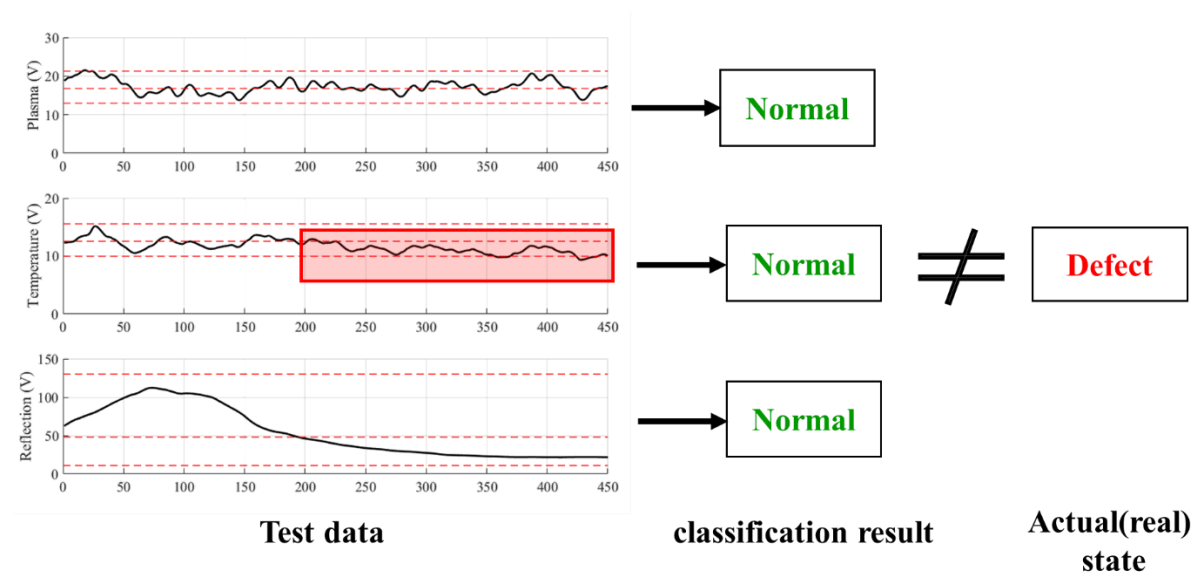


Figure 4-2 An illustration of in-tolerance failure problem

Third, the specific defect patterns of the signal may exist. It can be interpreted as a generalized version of multiple thresholds problem. As shown in this Figure 4-3, specific patterns can be extracted from the different sensor signal. How we can divide one signal to several pieces of segments, codify the segmented pieces, and interpret the series of the codified segment will be the approaches for the solution of this problem.

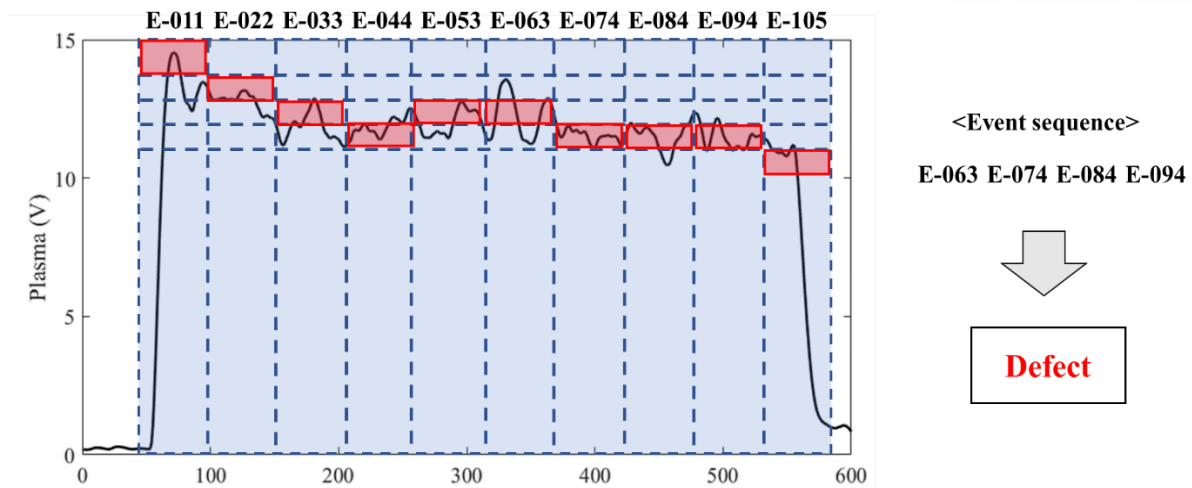


Figure 4-3 An illustration of event pattern classification and the segmentation problem

In this research, we focused on the first and the second issues by applying evidence theory and modified probability assignment function for detecting the weld defect from the multiple sensory information.

As shown in Figure 4-4, the defect detection system is divided into two processes. The first is training process to derive thresholds of normal status from the training data. The second is a testing process to detect or classify the testing event as a normal or abnormal status. This defect detection technique that operates in a semi-supervised model assumes that the training data has labeled instances for only the normal class.

Based on the Dempster-Shafer theory of inference, we were able to treat uncertainty of in-tolerance failure. The Dempster’s combination rule was used to combine multiple source information to overcome the first problem as we mentioned above.

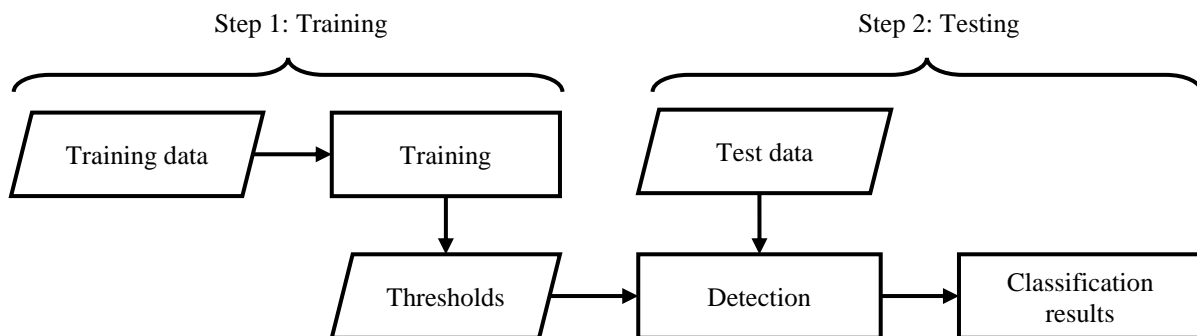


Figure 4-4 A process flow of the general fault detection system

4.2 Estimation of a probability distribution function for sensor data

The training process is to generate the threshold using previous training data for the testing hypothesis of normal status. In this case, we used three sensor signal data, which were plasma, temperature, and back-reflection of normal status. For generating threshold, normal state models of each sensor data were predicted.

Calculating the goodness of fit among the several probability models is compared to fit the best probability density function model of each sensor data. The goodness of fit is a degree of fitting between hypothesis and probability distribution function extracted from sensor data. It gives us the best-fitted probability distribution function with its estimated parameter values corresponding the data histogram gathered. In order to extract compatible probability distribution function from the data, criteria for degree of fit were needed such as NLogL(Negative of the log likelihood), AIC(Akaike information criterion), AICc(AIC with a correction for finite sample sizes), and BIC(Bayesian information criterion)(Oh and Kim, 2014). A probability distribution function with the smallest negative log likelihood value, among the different probability distribution function, was the best fit to the data. In the case of temperature signal, estimation of probability distribution function is shown Figure 4-5.

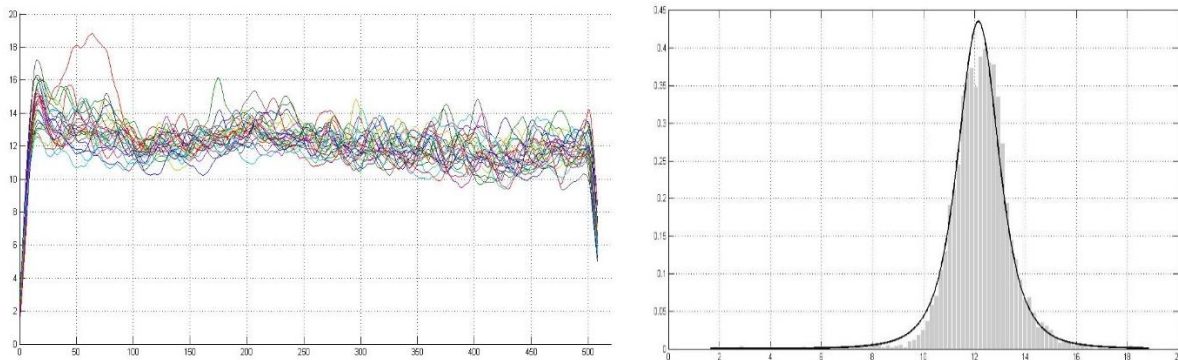


Figure 4-5 An example of PDF estimation result (Gamma distribution) of gathered temperature sensor data

The bold curve is Gamma distribution ($k=22.6594$ and $\theta=0.8923$) which was the best fit for the specific sample stitch. The distribution function scored the smallest NLogL value among the value of other probability distribution functions. Each sensor had a different estimation of probability

distribution function results. Once estimation of probability distribution function for each sensor was conducted, the statistical thresholds were generated by the distribution.

Algorithm 1. Estimation of Probability distribution function

Require: $\{g_1(\theta|x), g_2(\theta|x), \dots, g_n(\theta|x)\}$ is possible set of probability distribution functions where x is observation vector

- 1: **for** $i = 1 : n$
 - 2: compute $NLogL(g_i(\theta|x))$
 - 3: **endfor**
 - 4: $g_{fit}(x|\theta) = \underset{g_n(\theta|x)}{argmax}(NLogL(g_n(\theta|x)))$
 - 5: $LowerControlLimit = \underset{x}{arg}(g_{fit}(x|\theta) = 0.025)$, $midpoint = \underset{x}{arg}(g_{fit}(x|\theta) = 0.500)$,
 - 6: $UpperControlLimit = \underset{x}{arg}(g_{fit}(x|\theta) = 0.975)$
-

4.3 Proposed probability assignment

4.3.1. The Dempster-Shafer theory

The Dempster-Shafer theory was introduced by Arthur Dempster and developed by Glenn Shafer. The Dempster-Shafer theory (Shafer, 1992) was developed to overcome the limitation of conventional probability theory by applying uncertainty in evidence. The limitation of Bayesian inference was that we only have focused on only conclusions for inferring a single probability such as $p(x|y)$. As an aspect of the Dempster-Shafer theory, whereas, we can assign the distributing support probability to the union of proportions as well as to a proportion itself. By doing so, we can deal with the uncertainty of the information. In this manner, the Dempster-Shafer theory was considered a generalized Bayesian theory (Sentz and Ferson, 2002, Smets, 1993). The principles of the theory are described as follows.

We set the possible hypothesis which is called frame of discernment. it is the finite set of all possible subset of Θ . Once the frame of discernment is determined, we can assign the masses to all the power set of Θ , which is called basic probability assignment (BPA). the assignment function is a kind of mapping to a probability between 0 and 1 as equation (1).

$$\text{basic probability function } M: 2^\Theta \rightarrow [0,1] \quad (1)$$

Each element from the Θ is mutually exclusive. The proportion of all evidence is allocated to every subset of Θ . Note that the empty set(\emptyset) should be the probability of 0, which implies that one of the conclusions must be true. The mass value of A ($m(H)$) is proportion of all evidence that supports this element of the power set, where A is a member of the power set.

$$M(\emptyset) = 0 \quad (2)$$

$$\sum_{A \subset 2^\Theta} M(A) = 1 \quad (3)$$

The basic probability value of $M(A)$ is related only to the event A. There is no additional information on any subsets of A. each subset of A has, by definition, its own mass respectively. It is understood to be a measure of the belief that is committed exactly to hypothesis A.

Assigning the masses to all the possible subsets has advantages comparing with the Bayesian approach which is only assigning probabilities to single elements of Θ and not on elements of the powerset of the possible states. Dempster-Shafer's evidence theory can let us deal with the quantitative uncertainty of the hypothesis in the case that some sensors can distinguish between normal and defect state, while the others might not be able to provide any hints about the states.

The total belief of A represents the total amount of belief of A and is calculated by the sum of the masses of elements which are subsets of A. It is represented as a Belief function(Bel), which is defined by the equation (4). It gives the total belief committed to A: $Bel(A)$. The function signifies a quantitative measure of one belief of evidence, which reflects the minimum belief value on A.

A Bel is a belief measure that maps the power set 2^Θ to the unit interval and is defined as follows:

$$Bel(A) = \sum_{B \subset A} m(B) \quad (4)$$

$$Bel(A) + Bel(\neg A) \leq 1 \quad (5)$$

where $\neg A$ is the complement of A.

A Plausibility, which is represented as $Pls(A)$ reflects the total amount of belief(the maximum belief) that could include potential evidence of A.

$$Pls(A) = \sum_{B \cap A \neq \emptyset} m(B) \quad (6)$$

$$Pls(A) = 1 - Bel(\neg A) \quad (7)$$

The equation (7) implies that the less compatible evidence of A, the more plausible it is.

The real belief in A lies between $Bel(A)$ and $Pls(A)$. As a result, uncertainty, more concretely ignorance, regarding A is represented by the difference of the two measures; $Pls(A) - Bel(A)$. The relationship between two measures are shown as Figure 4-6.

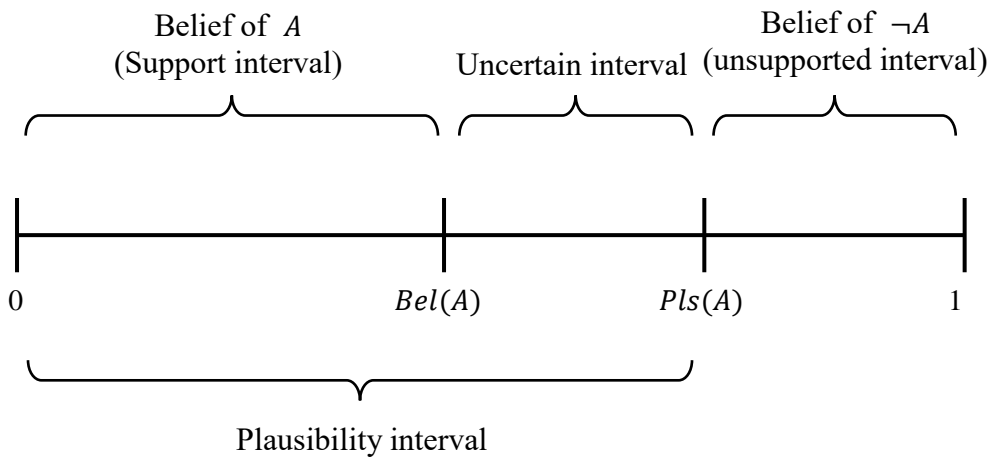


Figure 4-6 The relation between $Bel(A)$ and $Pls(A)$

4.3.2. The thresholds adaptive probability assignment function

Probability distribution functions were estimated by using good-welded signals. The best-fitted probability distribution function was selected in accordance with the lowest value of $N\log L$ (Negative log likelihood). The best-fitted probability distribution function is divided into three intervals corresponding the probability of 2.5% (lower control limit), 50% (midpoint), 97.5% (upper control limit) respectively.

The probability assignment was conducted based on the generated thresholds from the training process.

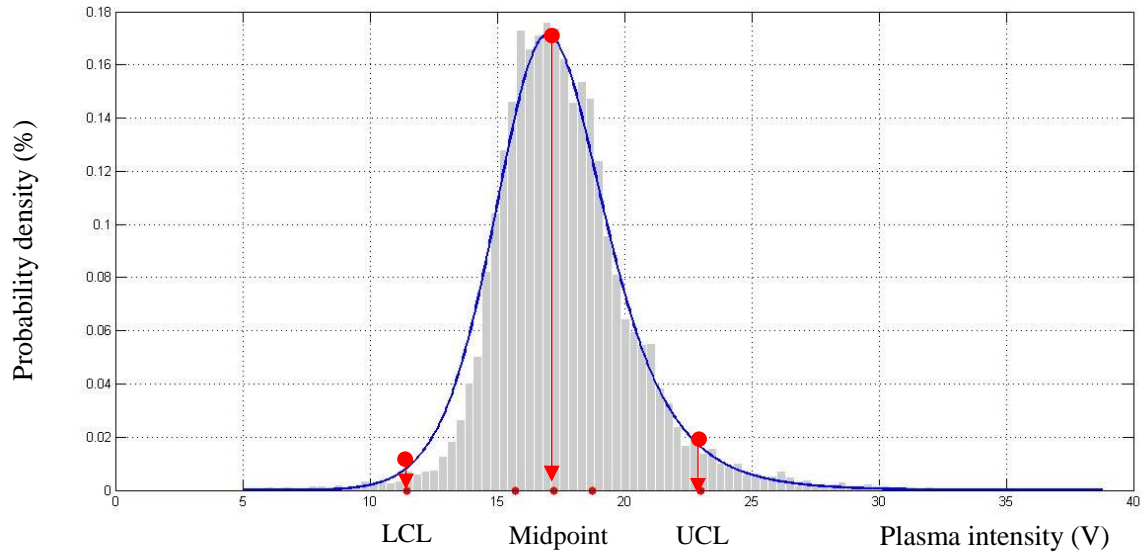


Figure 4-7 A best-fitted probability distribution function of plasma intensity signal

We assumed that the value between lower and upper control limit tends to be the normal state based on the estimated probability model. If current sensor signal level is larger than the upper control limit or smaller than the lower control limit, the probability of being a normal state decreased. Chen and Aickelin (Chen and Aickelin, 2006) implemented an anomaly detection system to evidence theory. They adopted standard sigmoid function to their anomaly detection algorithm to analyze the Wisconsin Breast Cancer Dataset (WBCD), which is widely used dataset for benchmarking of fault detection methods (Goldstein and Uchida, 2016). They utilized the function as a basic probability assignment function(activation function).

We defined a modified version of the dual sigmoid function(equation (8) and (9)) to control the slope of the probability function for gradual changes around the thresholds. The exact equation of the proposed adaptive probability assignment function is:

$$M_{paf}(H) = \begin{cases} (1 + e^{slopeCoeff*(datapoint-UCL)})^{-1}, & datapoint \geq midpoint \\ (1 + e^{-slopeCoeff*(datapoint-LCL)})^{-1}, & otherwise \end{cases} \quad (8)$$

where

$$slopeCoeff = \frac{UCL + LCL}{UCL - LCL} \quad (9)$$

It illustrated that the probability of a hypothesis which is a current state is normal. A slopeCoeff controls and adjusts the proposed probability assignment function by changing the slope of the graph

near the thresholds. The difference between upper and lower control limit is getting larger, slopeCoeff is getting larger, which result in the steeper slope of the probability function nearby the upper and lower control limits. A simple comparison of the probability assignment function with respect to the different slopeCoeff is illustrated in Figure 4-8. It illustrated how the coefficient adjusts and controls the slope of the probability assignment functions.

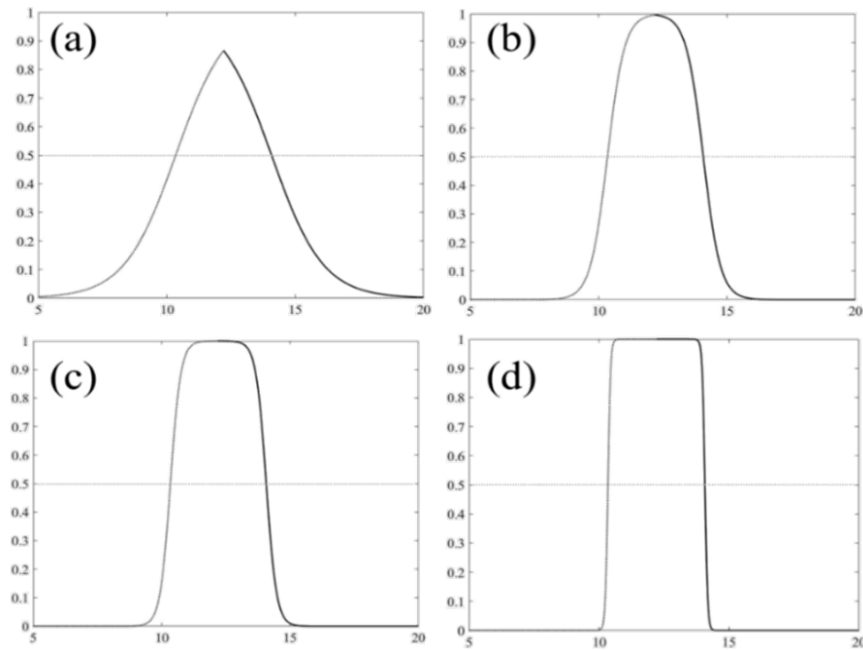


Figure 4-8 A comparison of proposed probability assignment function with respect to the magnitudeCoeff: (a) 1, (b) 3, (c) 5, (d) 20

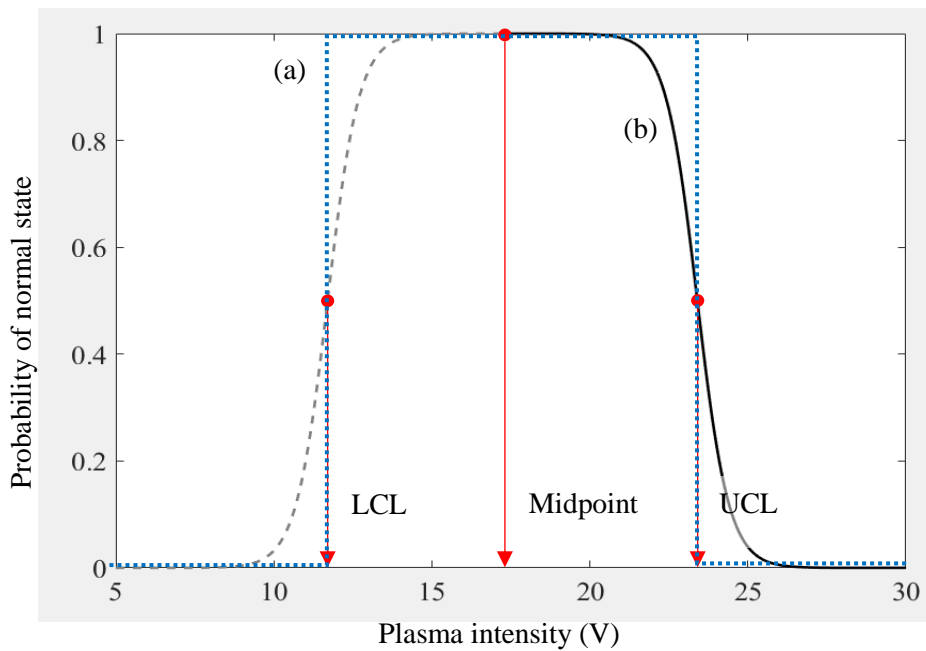


Figure 4-9 An example of the adaptive probability assignment function of upper control limit: 23.4V, lower control limit: 11.7V, and midpoint:17.3V

Traditionally, a binary decision approach based on the statistical analysis is shown in the Figure 4-9 (a). It implies that the decision model classifies the current weld status as a defect state if the current voltage is out of the thresholds range between the LCL and UCL. However, the binary categorical classification was unable to handle the uncertainty in terms of the in-tolerance failure problem.

To solve the problem, we defined a new probability assignment function by assigning the gradually decreasing probability of normal state nearby the thresholds. A graphical illustration of the probability assignment function with thresholds(in this case of the plasma signal, upper control limit: 23.4V, lower control limit: 11.7V, and midpoint:17.3V) is shown in Figure 4-9 (b).

The proposed probability assignment function was quite reasonable to consider the uncertainty around the thresholds. We further improved the proposed probability assignment function by adding the information of the estimated probability density function from chapter 4.3.1. The weighted summation of the two probability information(The estimated probability density function and The proposed probability assignment function) was used to assign the probability of the normal state. The weight(α) was selected as an arbitrary value from the pre-experiments. The weight decided how much the amount of information from the estimated probability density function would be adjusted to the proposed probability assignment function. By applying the weight, the probability assignment function contains richer information in terms of skewness of the original training data.

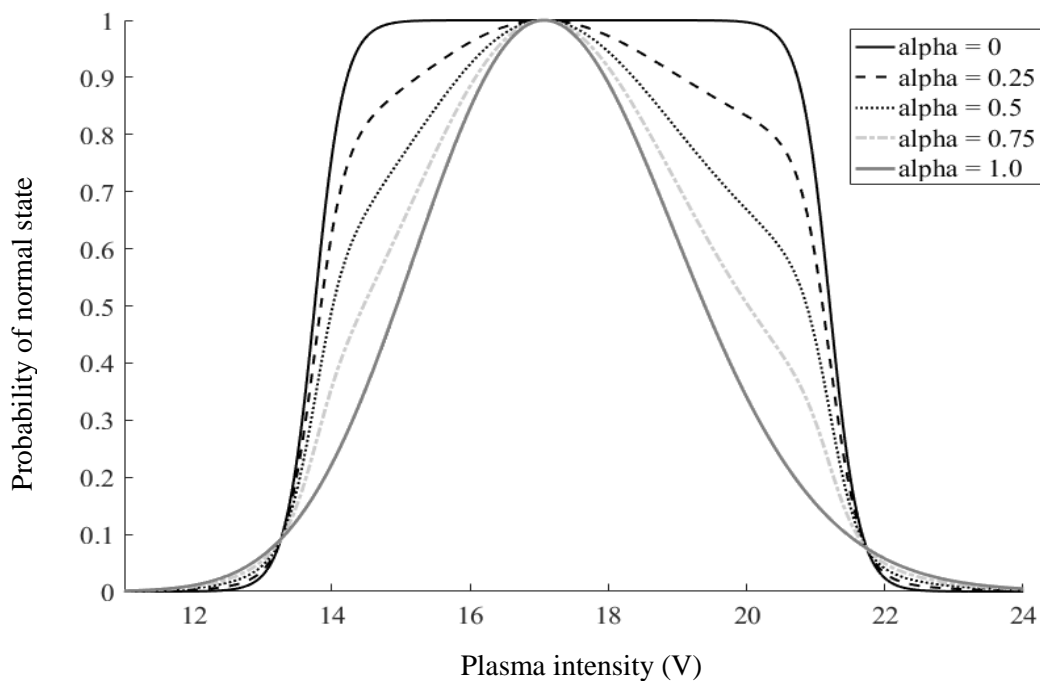


Figure 4-10 A comparison of the adjusted probability assignment function with respect to the different weights(α): “ $\alpha=0$ ” implies that there is no further information of the estimated probability density function

The detailed equation for the adjusted probability assignment function is described as equation (10).

$$M_{sensor}(H) = \alpha * g_{fit}(H) + (1 - \alpha) * M_{paf}(H) \quad (10)$$

Further, we have to assign a value to the set $\{H, \neg H\}$ to express the ignorance of the sensor and the possibility that might be uncertain to determine whether the current state is normal or not; $M(H, \neg H) \rightarrow [0, 1]$.

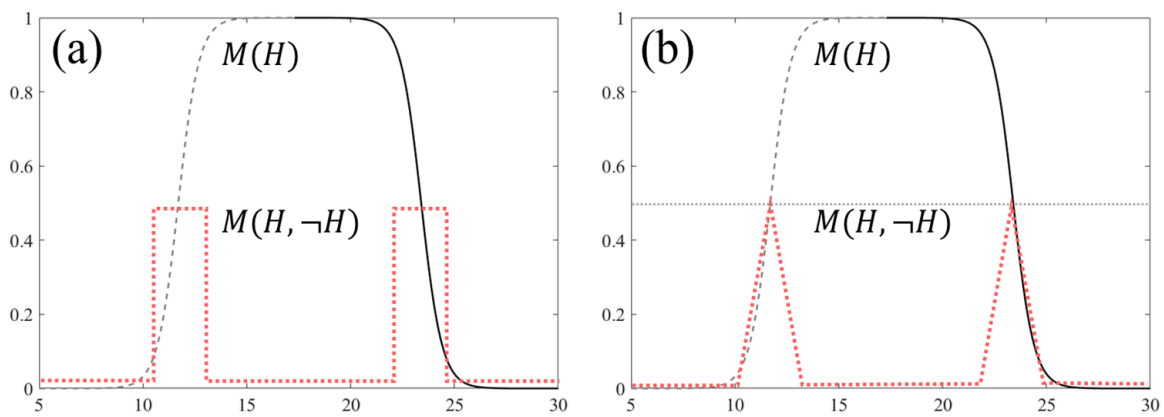


Figure 4-11 A general guideline to define basic probability assignments of dual threshold interval(a) and modified probability assignment of $M(H, \neg H)$

A general guideline to define the $M(H, \neg H)$ is shown in Figure 4-11(a)(Siaterlis and Maglaris, 2004). The intuition behind this ‘general guideline’ is that the decision beliefs should be treated with an uncertainty at the transient state even though the thresholds provide a quite certain decision.

From the Siaterlis and Maglaris research, we also modified the guidelines for assigning the ignorance as shown in Figure 4-11(b). The level of uncertainty given by $M(H, \neg H)$ gradually increases or decreases at the transient state of the graph(see Figure 4-11(b)), denoting the sensor's uncertainty related to the value of $M(H)$.

We followed the equation that $M(H) + H(\neg H) + H(H, \neg H) = 1$ to assign a probability of $H(\neg H)$.

Algorithm 2. Threshold adaptive probability assignment

Require:*ucl_S* = upper control limit of sensor *S**lcl_S* = lower control limit of sensor *S**mp_S* = midpoint of sensor *S**x_{Si}* = *i*th datapoint of sensor *S**slopeCoeff_S* = magnitude coefficient of sensor *S**α_S* = weight value of sensor *S**M_{Si}(H)* = proposed probability distribution assignment function of sensor *S* with *i*th datapoint when hypothesis *H* is true1: **for** *S* = 1 : number of sensors2: **for** *i* = 1 : number of data point on a stitch3: **if** *x_{Si}* ≥ *mp_S* **then**

4:
$$M_{S_paf_i}(H) = \frac{1}{1 + \exp(\text{slopeCoeff}_S * (x_{Si} - UCL_S))}$$

5: **else**

6:
$$M_{S_paf_i}(H) = \frac{1}{1 + \exp(-\text{slopeCoeff}_S * (x_{Si} - LCL_S))}$$

7: **end if**

8:
$$M_{S_paf_i}(H) = \frac{1}{1 + \exp(\text{slopeCoeff}_S * (x_{Si} - UCL_S))}$$

9:
$$M_{Si}(H) = \alpha_S * g_{fit}(x_{Si} | \theta) + (1 - \alpha_S) * M_{S_paf_i}(H)$$

8: **if** *M_{Si}(H)* ≥ 0.5 **then**

9:
$$M_{Si}(H, \neg H) = 1 - M_{Si}(H)$$

10: **else**

11:
$$M_{Si}(H, \neg H) = M_{Si}(H)$$

12: **end if**

13:
$$M_{Si}(\emptyset) = 0$$

14:
$$M_{Si}(\neg H) = 1 - M_{Si}(H) - M_{Si}(H, \neg H)$$

15: **end for**16: **end for**

4.4 Multi-sensor evidence fusion by the Dempster's combination rule

The data from the several information sources were calculated and allocated by corresponding modified probability assignment functions. The probability assignment function from different sensors was fused as one criterion by the Dempster's rule of combination (Shafer, 2016, Shafer, 1976)(also called orthogonal sum rule).

Assume that there are two information sources such as plasma, and temperature sensors. Suppose that the plasma detector believes the hypothesis H (Normal) is true with confidence of $M_T(H)$, and temperature detector believes the hypothesis H (Normal) is true with confidence of $M_P(H)$. Dempster-shafer's combination rule, which is symbolized as \oplus , can combine the two separate beliefs into a single belief as formula below:

$$M_{combined}(H) = (M_P \oplus M_T)(H) = \frac{\sum_{B \cap C = A} M_P(B) * M_T(C)}{1 - K} \quad (11)$$

where

$$K = \sum_{B \cap C = \emptyset} M_P(B) * M_T(C) \quad (12)$$

The denominator of equation (11) can be interpreted as a kind of normalization factor for combination result of belief $M_P \oplus M_T(H)$. K in formula represents a probability value related to the measure of conflict between the combining sources when M_P and M_T is combined in terms of event A . A conflict can appear when, for example, plasma detector has a strong belief on H whereas temperature detector has a strong belief on $\neg H$. Consequently, The smaller the value of denominator is, the more conflict exists between two sources, and the less informative is after the fusion.

Table 4-1 Dempster's combination table for the two basic probability functions

$M_P(x) \backslash M_T(x)$	H	$\neg H$	$H, \neg H$
H	$M_{combined}(H)$ $= M_P(H) * M_T(H)$	$M_{combined}(\emptyset)$ $= M_P(\neg H) * M_T(H)$	$M_{combined}(H)$ $= M_P(H, \neg H) * M_T(H)$
$\neg H$	$M_{combined}(\emptyset)$ $= M_P(H) * M_T(\neg H)$	$M_{combined}(\neg H)$ $= M_P(\neg H) * M_T(\neg H)$	$M_{combined}(\neg H)$ $= M_P(H, \neg H) * M_T(\neg H)$
$H, \neg H$	$M_{combined}(H)$ $= M_P(H) * M_T(H, \neg H)$	$M_{combined}(\neg H)$ $= M_P(\neg H) * M_T(H, \neg H)$	$M_{combined}(H, \neg H)$ $= M_P(H, \neg H) * M_T(H, \neg H)$

We can convert the equation (11) to a matrix form for calculating the combination rule.

The combined belief of normal state is calculated by summation of $M_{combined}(H)$. The total summation of $M_{combined}(H)$ and $M_{combined}(H, \neg H)$ denotes the combined probability of $M(H)$ and $M(H, \neg H)$.

$$Bel(H) = M_P(H) * M_T(H) + M_P(H) * M_T(H, \neg H) + M_P(H, \neg H) * M_T(H) \quad (13)$$

$$Pls(H) = Bel(H) + M_P(H, \neg H) * M_T(H, \neg H) \quad (14)$$

In this case of $\Theta = \{H, \neg H\}$, all the power set of frame of discernments, which is $\{\emptyset, H, \neg H, \{H, \neg H\}\}$, are mapped in the form of two binary digits respectively for the bitwise conjunctive operation(AND) computation for the combination procedure. The mapped binary values are represented as the Table 4-2. A set of all possible subset of assigned basic probability(mass function) is converted to vector form to compute vector inner product computation.

Table 4-2 Boolean truth table for the combination of two basic probability function

$M_P(x) \backslash M_T(x)$	$H: (01)_2$	$\neg H: (10)_2$	$H, \neg H: (11)_2$
$H: (01)_2$	$(01)_2$	$(00)_2$	$(01)_2$
$\neg H: (10)_2$	$(00)_2$	$(10)_2$	$(10)_2$
$H, \neg H: (11)_2$	$(01)_2$	$(10)_2$	$(11)_2$

The detailed multisensor fusion algorithm in this thesis is as follows:

Algorithm 3. Sensor fusion algorithm based on the Dempster's combination rule

Require:

$x_i = [\emptyset, H, \neg H, \{H, \neg H\}]$: *ith proposed probability assignment row vector*

$Map_{dec2bi}(X)$ = *mapping fuction of matrix index to binary digits*

combiMatrix = Dempster's combination matrix (dot product of two vectors)

1: $combiVec = x_1$

2: **for** $i = 1 : n-1$

3: $combiMatrix = combiVec * x_{i+1}'$

4: $M_{combined}(H) = sum(combiMatrix \text{ where } Map_{dec2bi}(combiMatrix) = "01")$

5: $M_{combined}(\neg H) = sum(combiMatrix \text{ where } Map_{dec2bi}(combiMatrix) = "10")$

6: $M_{combined}(H, \neg H) = sum(combiMatrix \text{ where } Map_{dec2bi}(combiMatrix) = "11")$

7: $combiVec = [0, M_{combined}(H), M_{combined}(\neg H), M_{combined}(H, \neg H)]$

10: **end for**

11: $Bel(H) = combiVec[M_{combined}(H)]$

12: $Pls(H) = combiVec[M_{combined}(H)] + combiVec[M_{combined}(H, \neg H)]$

The combination rule satisfies the law of commutativity and associativity. The combination of more than three sources, and thus, can be calculated as follows:

$$M_P \oplus M_T \oplus M_R(H) = ((M_P \oplus M_T) \oplus M_R)(H) \quad (15)$$

The state of current weld result is classified by testing combined belief is larger than a certain threshold(user selected).

A whole procedure for the defect detection system including the combination of each evidence (basic probability mass value) is illustrated as follows in Figure 4-12. The normal state data from three sources are pre-processed and trained as a form of a threshold. Based on the thresholds and basic probability assignment functions, test data are determined the probability of the normal state. The probability vectors came from the different information sources are combined by Dempster's combination rule.

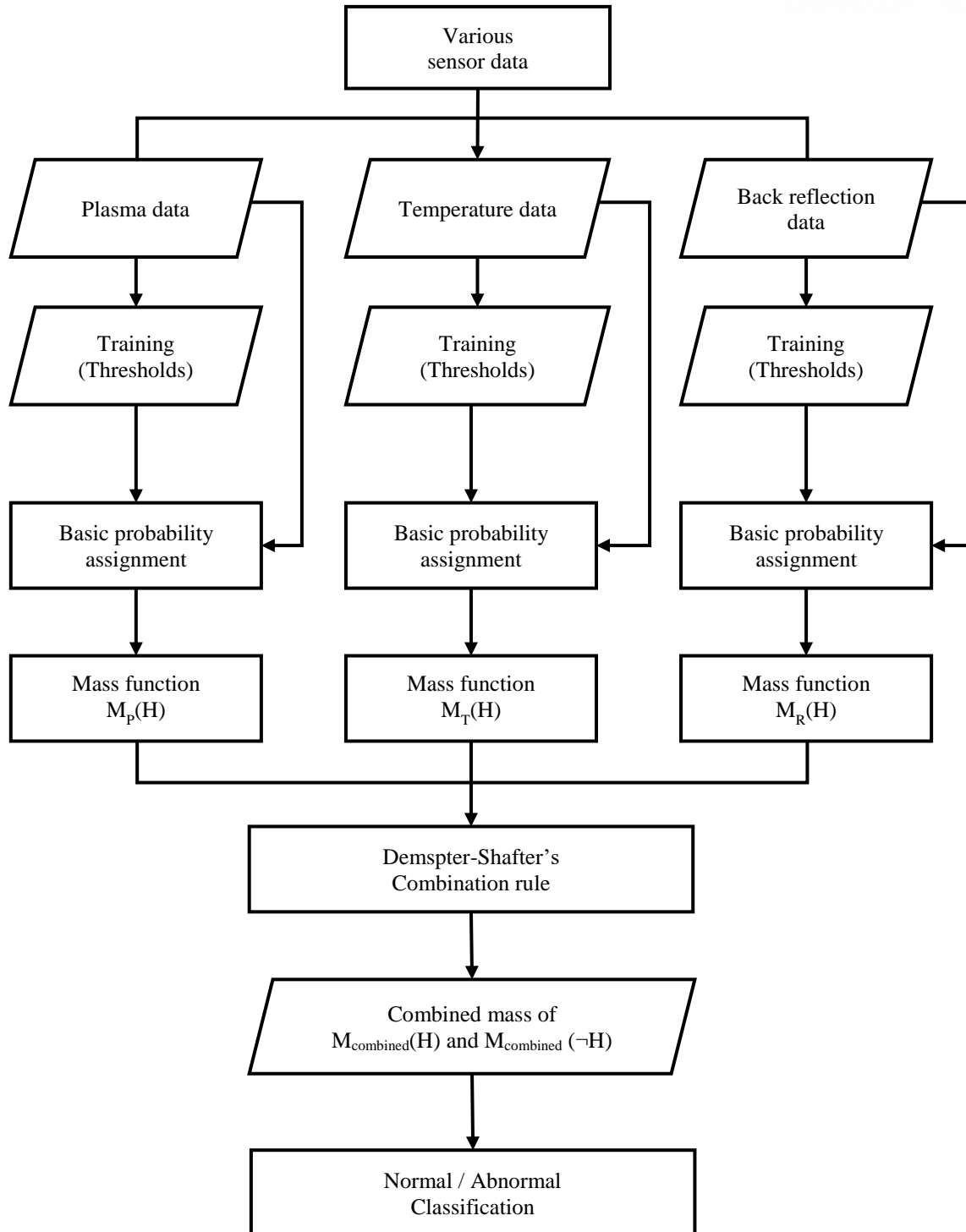


Figure 4-12 A procedure of the defect detection system with the sensor fusion of each evidence

4.5 Problem sets

A series of experiments have been conducted to validate and verify the proposed weld defect detection method of this thesis.

4.5.1 Experimental setup

We performed coupon tests with the 6-kW disk laser and 2-kW fiber laser welding system to statistically verify the proposed defect detection method and the sensor fusion method.

Figure 4-13 shows a schematic representation of the experimental setup. As shown in this Figure 4-13 (a), thickness gauges of 0.2mm and 0.3mm were used to retain the appropriate part-to-part gap between two steel sheets for ventilating the zinc vapor. The only difference between the Figure 4-13 (a) and (b) is whether the part-to-part gap was inserted at the last stitch or not. The weld defects were caused by the intentionally removed part-to-part gap. We used (a) and (b) as a setup for the experiment #1 and #2. In the case of the experiment #3 and #4, experimental setup (a) and (c) were utilized.

The experimental materials used were dual-phase steel, both of which are galvanized with a zinc coating layer; 1.4-mm-thick (upper part) SG AFC590DP and 1.8-mm-thick (lower part) SG ARC440, which have been used in car side-member parts. The amount of zinc coating on the lower and upper parts and their chemical compositions and mechanical properties of the tested materials are summarized in Table 4-3.

All the specimens and thickness gauges were cleaned using an alcohol cleaner to remove any dust and oil layers, and the specimen was tightly clamped on each side of the stitch to minimize any unexpected part-to-part gaps.

Based upon the experimental data, the proposed weld defect detection and combination rule was tested as the performance measure of precision, recall and F-score.

Table 4-3 Chemical composition of experimental specimen (galvanized steel)

Material	Thickness (mm)	C (%)	Si (%)	Mn (%)	P (%)	S (%)
SG AFC 590DP lower part	1.8	0.09	0.26	1.79	0.03	0.003
SG ARC 440 upper part	1.4	0.08	0.02	1.38	0.02	0.003

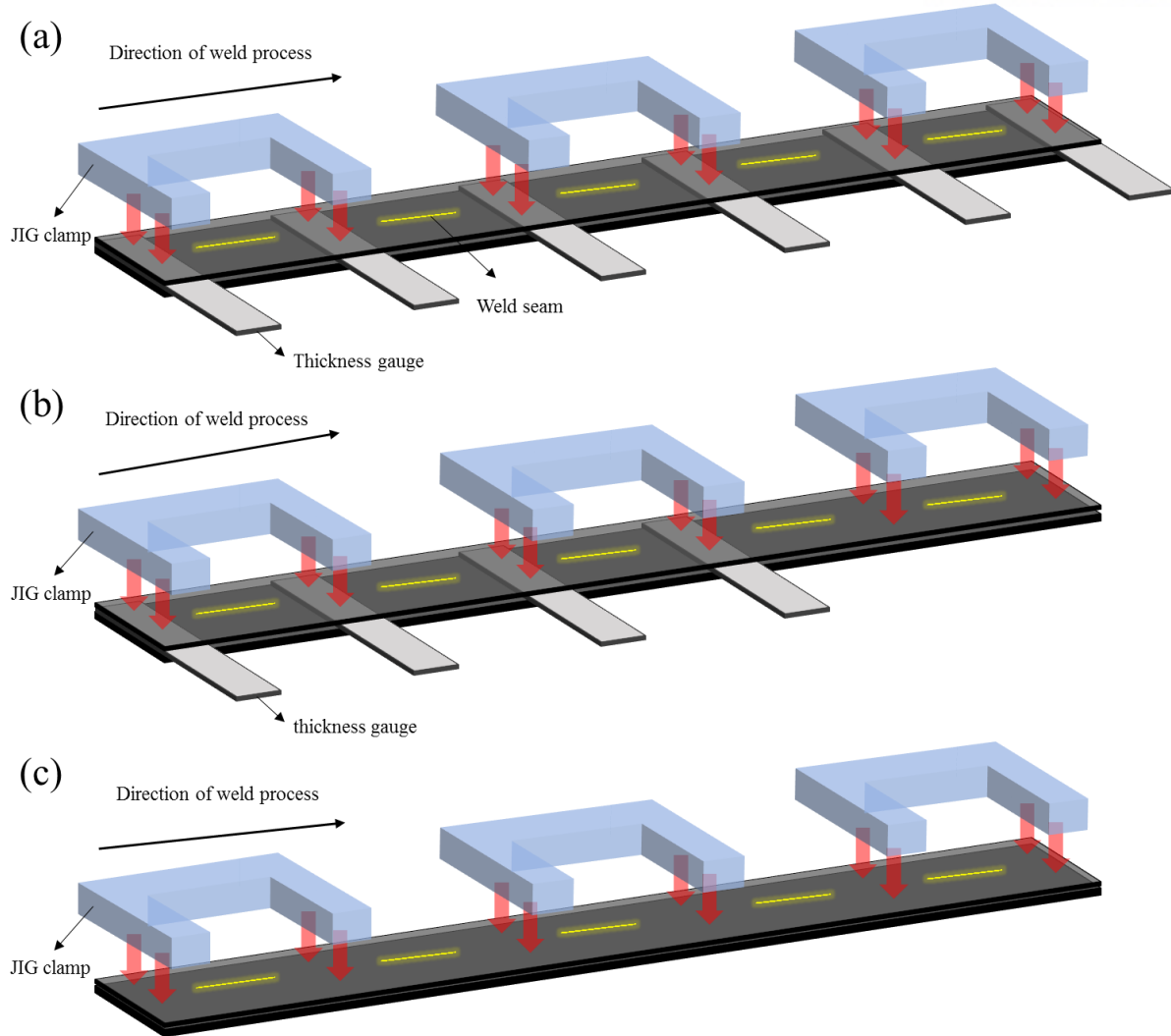


Figure 4-13 Experimental setup

Table 4-4 Laser welding process parameter for the experiments

Experiment	Stitch length (mm)	Feed rate (mm/min)	Laser power (kW)	Part-to-part gap (mm)
#1 6.6kW disk laser	30	3600	5.0	0.2
#2 6.6kW disk laser	30	3600	5.0	0.3
#3 2kW fiber laser	30	900	2.0	0.2
#4 2kW fiber laser	30	900	2.0	0.3

4.5.2 Experimental result and discussion

We conducted the four experiments above. The total dataset of the four experiments were 50, 45, 100, 105 respectively. The actual defects were classified by the visual inspection rule defined in Chapter 3. The number of actual defects occurred and good weld result is summarized in Table 4-5. We then analyzed the experimental data and validated the proposed weld defect detection with the sensor fusion method(Dempster's combination rule). The actual defects were compared the result of the proposed weld defect detection results. The defect detection accuracy was calculated as the more sensors information(data) were fused.

In the case of weld defect detection regime, the proportion of the actual states (normal and abnormal) is highly skewed. This characteristic of dataset makes it hard to determine the performance of the proposed detection method. A comparison of accuracy(error rate), which is calculated as a proportion of correct detections, is not enough to measure the performance due to the lack of abnormal data(Thomas and Balakrishnan, 2008). This traditional performance measure is not adequate while dealing with states(classes) which are very rare. In this case, precision, recall, and F-score are suitable indexes for the performance of the detection method (Patcha and Park, 2007).

Precision is a measure of what fraction of the test data detected as normal is actually from the normal state. Recall, on the other hand, is a measure of what fraction of the normal state is correctly detected. There is a trade-off between the precision and recall. As the detection threshold is getting larger, the better precision is. The recall, on the other hand, is being worse. It is, thus, required to evaluate how it performs better on both recall and precision. F-score, which can be considered as the harmonic mean of recall and precision, is finally used to measure the performance of proposed detection method. As shown in the equation (18), a higher value of F-score indicates that the proposed method is performing better on recall as well as precision.

Table 4-5 The number of actual defected samples in the experiment #1 ~ #4

Experiment	Normal	Defect	Total number of samples
#1 6.6kW disk laser	45	5	50
#2 6.6kW disk laser	40	5	45
#3 2kW fiber laser	61	39	100
#4 2kW fiber laser	66	39	105

Table 4-6 Confusion matrix

		Actual defect	
		True	False
Predicted result	True	True positive	False positive
	False	False negative	True negative

$$Precision = \frac{True\ Positive}{True\ positive + False\ positive} \quad (16)$$

$$Recall = \frac{True\ Positive}{True\ positive + False\ Negative} \quad (17)$$

$$F - score = \frac{2 * Precision * Recall}{Precision + Recall} \quad (18)$$

The weld defect detection results of the four experiments are shown in Figure 4-14 ~ Figure 4-17. From the experimental results, we observed that the sensor fusion of plasma and temperature signal gave the better accuracy regarding the F-score metric rather than just using individual sensors for defect detection.

The sensor fusion, however, did not always provide the better detection accuracy as shown in Table 4-9 and Table 4-10. As shown in the tables, sensor fusion with reflection signal resulted in the worse performance of F-score. The sensor fusion of all three sensors(plasma, temperature, and reflection) also decreased the f-score compared to the F-score of sensor fusion of temperature and plasma signal.

Even though the F-score decreased when reflected signal was fused, the lower bound of accuracy increased by fusing other sensors with the reflected signal. The retaining the robustness is one of the advantages of sensor fusion. The result provided some evidence that the fusion of qualified information sources improved the reliability of weld defect detection accuracy.

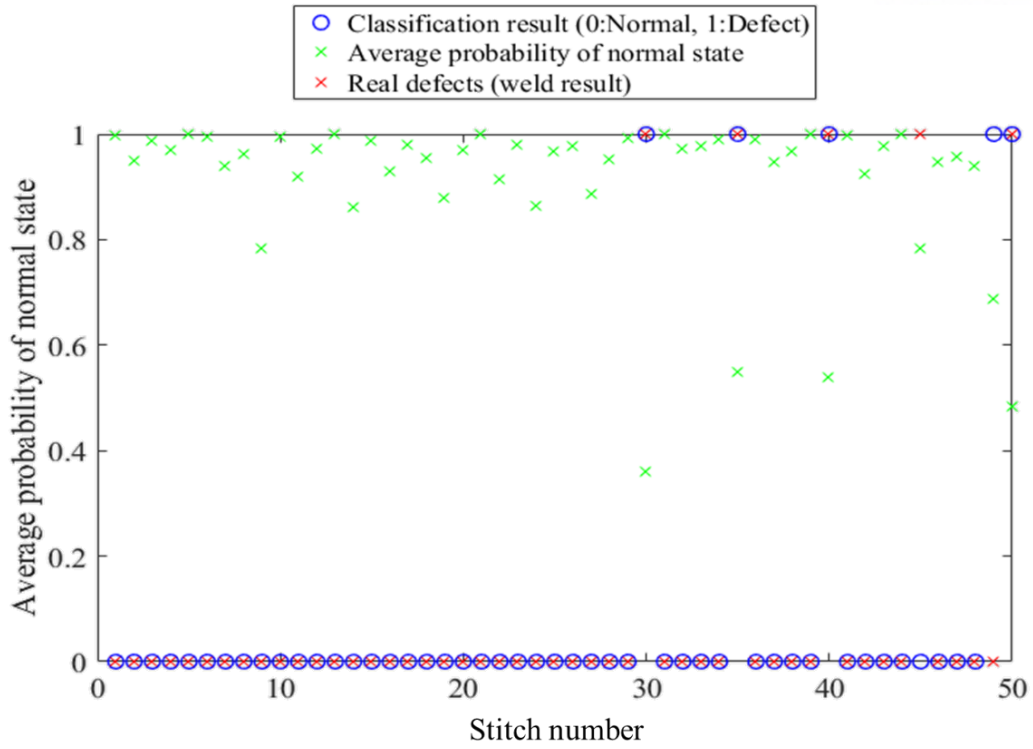


Figure 4-14 Average probability of normal state and corresponding classification result of experiment #1

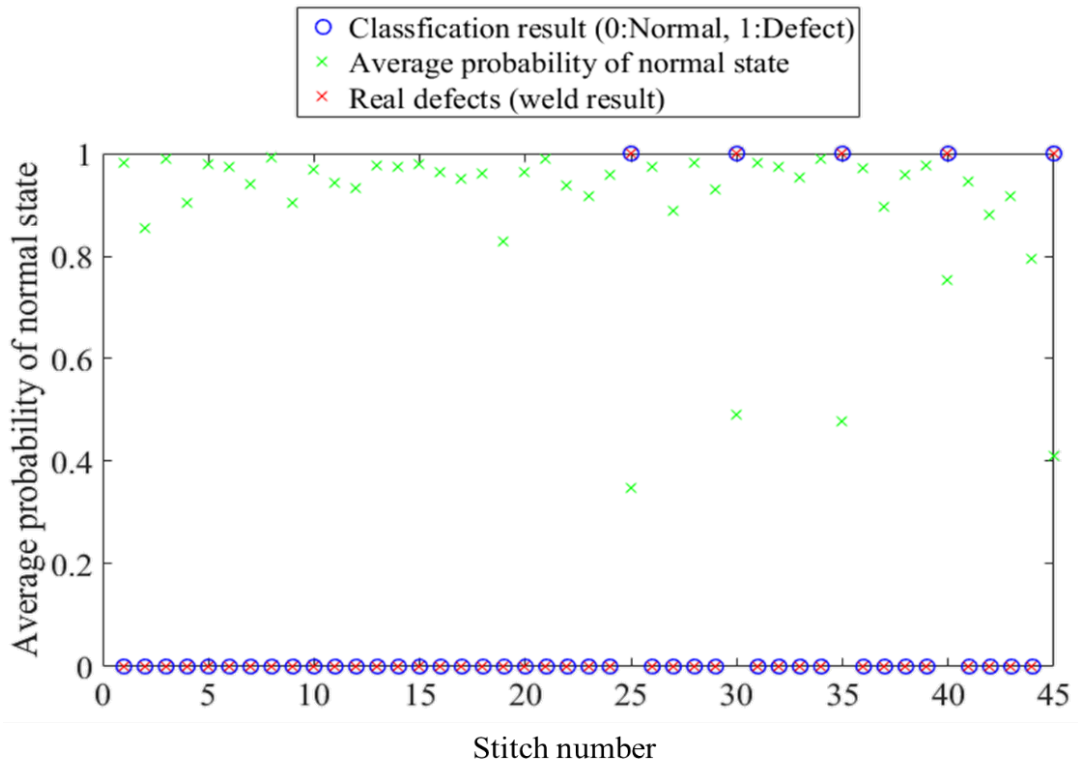


Figure 4-15 Average probability of normal state and corresponding classification result of experiment #2

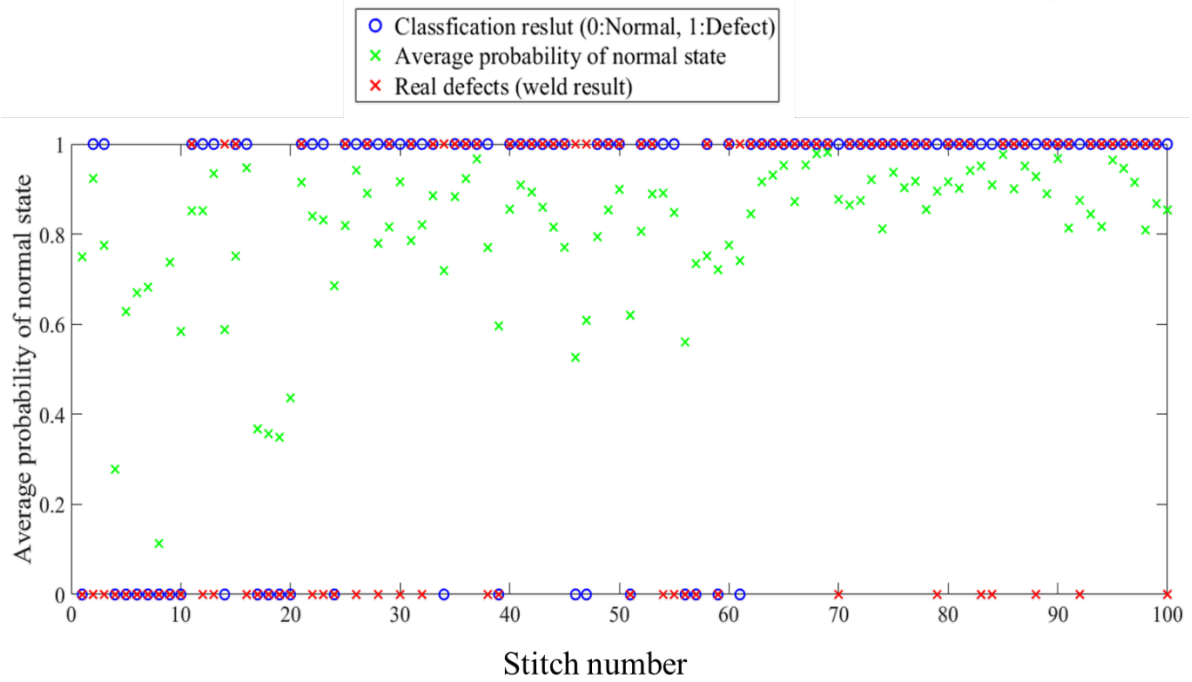


Figure 4-16 Average probability of normal state and corresponding classification result of experiment #3

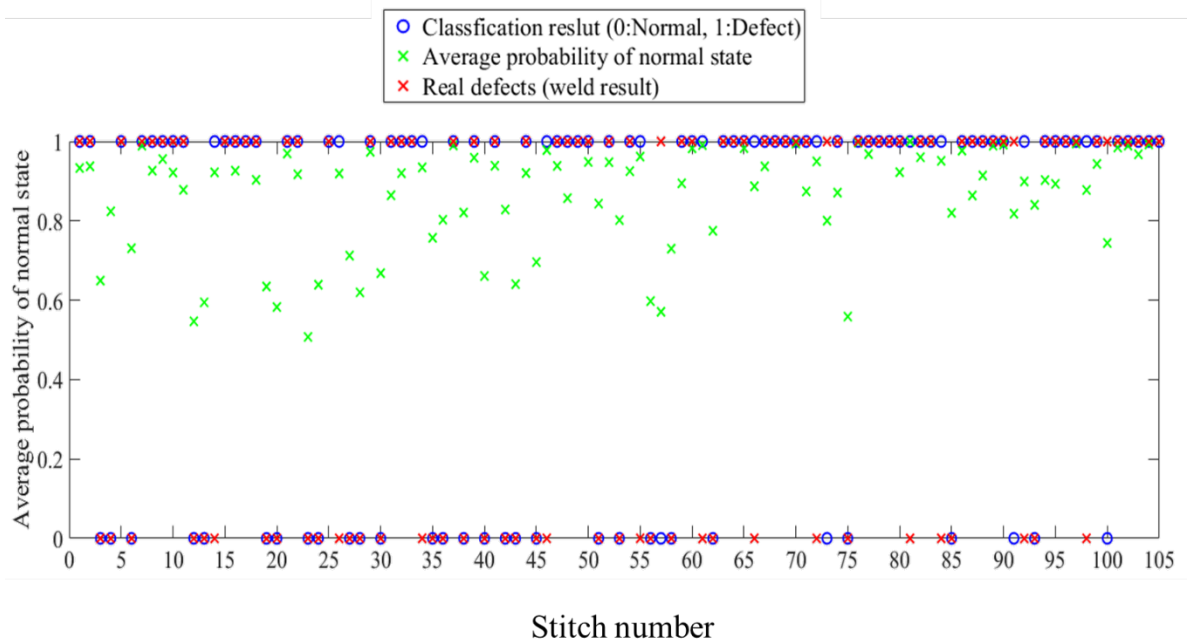


Figure 4-17 Average probability of normal state and corresponding classification result of experiment #4

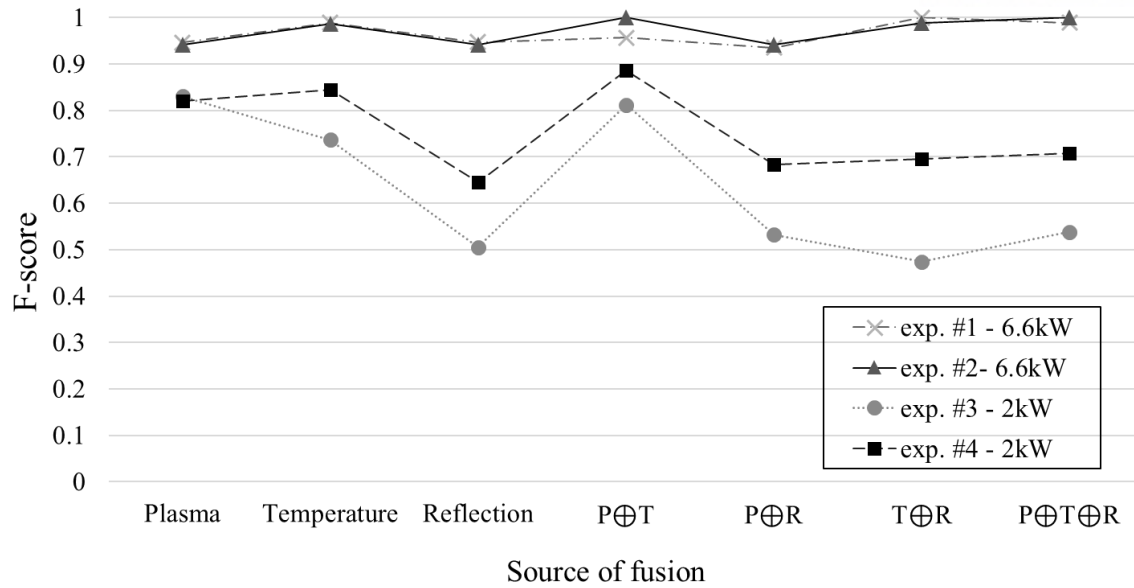


Figure 4-18 A comparison of the F-scores corresponding the number of sources for sensor fusion

Table 4-7 The performance metrics (precision, recall, and F-score) of the experiment #1

Sources of multisensory fusion	Precision	Recall	F-score
Plasma signal	0.978	0.917	0.946
Temperature signal	0.978	1.000	0.989
Reflection signal	1.000	0.900	0.947
Plasma + Temperature	0.978	0.936	0.957
Plasma + Reflection	0.956	0.915	0.935
Temperature + Reflection	1.000	1.000	1.000
Plasma + Temperature + Reflection	1.000	0.978	0.989

Table 4-8 The performance metrics (precision, recall, and F-score) of the experiment #2

Sources of multisensory fusion	Precision	Recall	F-score
Plasma signal	1.000	0.889	0.941
Temperature signal	0.975	1.000	0.987
Reflection signal	1.000	0.889	0.941
Plasma + Temperature	1.000	1.000	1.000
Plasma + Reflection	1.000	0.889	0.941
Temperature + Reflection	1.000	0.976	0.988
Plasma + Temperature + Reflection	1.000	1.000	1.000

Table 4-9 The performance metrics (precision, recall, and F-score) of the experiment #3

Sources of multisensory fusion	Precision	Recall	F-score
Plasma signal	0.918	0.757	0.830
Temperature signal	0.918	0.615	0.737
Reflection signal	0.410	0.658	0.505
Plasma + Temperature	0.918	0.727	0.812
Plasma + Reflection	0.410	0.758	0.532
Temperature + Reflection	0.377	0.639	0.474
Plasma + Temperature + Reflection	0.410	0.781	0.538

Table 4-10 The performance metrics (precision, recall, and F-score) of the experiment #4

Sources of multisensory fusion	Precision	Recall	F-score
Plasma signal	0.970	0.711	0.821
Temperature signal	0.985	0.739	0.844
Reflection signal	0.591	0.709	0.645
Plasma + Temperature	0.939	0.838	0.886
Plasma + Reflection	0.591	0.813	0.684
Temperature + Reflection	0.606	0.816	0.696
Plasma + Temperature + Reflection	0.621	0.820	0.707

We analyzed that the reason for the accuracy decreased in fusion with reflection signal information. As shown in Figure 4-19, We rearranged the gathered signal as an order of experimental time sequence. The mean voltage of the reflection signal had a strong time-dependent relation. The reflection signal tended to be closely related to the temperature of the laser source. As the experiment was conducted, the temperature of laser source itself increased from 20° to 25°. In this manner, the mean value of the reflected laser signal gradually increased. Also, the baseline of the reflected signal was different depending on the target stitches. It implies that gathering the reflected signal should be treated differently by stitches. We need to train the thresholds for defect detection stitch by stitch. If we gathered reflected signal of the stitch-1, for example, estimation of the probability distribution should be conducted by using the set of stitch-1 signal data. The two factors increased the error rate of the proposed defect detection algorithm.

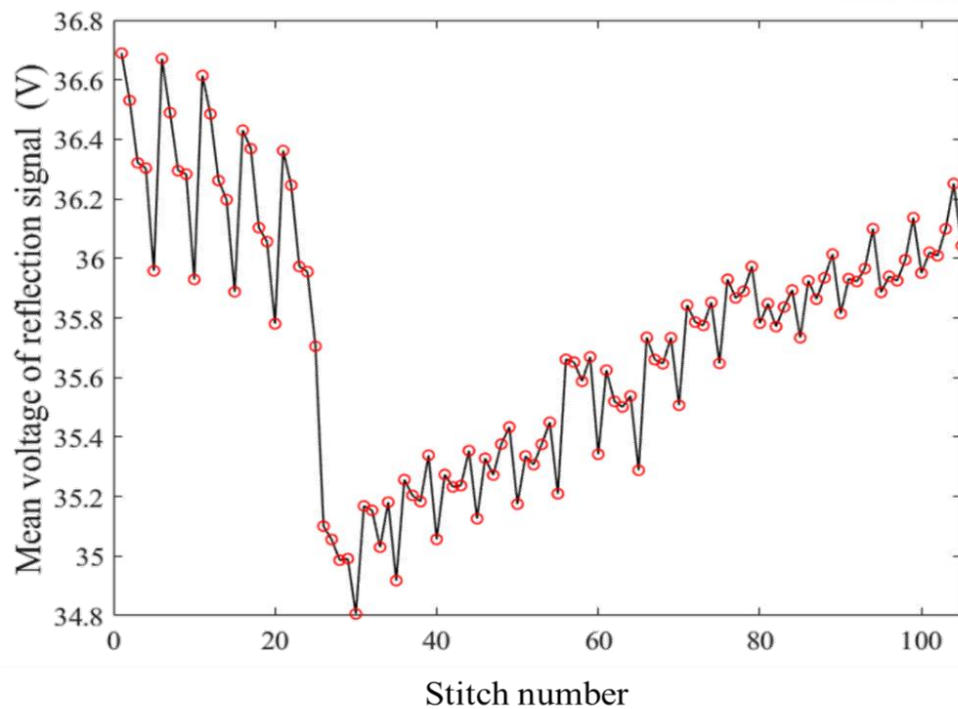


Figure 4-19 Mean voltage of reflection signal at each stitch

We further conducted sensitivity analysis by changing the weight value(α) and confidence interval(β) from threshold extraction step. The detection threshold for the final decision and classification is also one of the essential parameters.

Even though we increased the weight value(α) from 0 to 0.75, the result of the analysis(see Figure 4-20) indicates that the weight(α) has no statistically significant effect on the highest F-scores under the condition of fixed confidence interval(0.95) for extracting UCL and LCL. As the weight(α) decreased, the decision threshold range for ensuring the F-score larger than 0.8 was expanded as shown in Figure 4-20. It means that the sensitivity of selecting the decision threshold was lessened by decreasing the weight(α).

The Figure 4-21 illustrated the response surface of the highest F-scores with respect to the weight and confidence interval. The F-score increased as the confidence interval was increased to 0.95. In the case of the confidence interval of 0.6 and 0.7, the F-score increased as the weight was increased to 0.7. There was no statistical difference between the different weights where the confidence level was larger than 0.8.

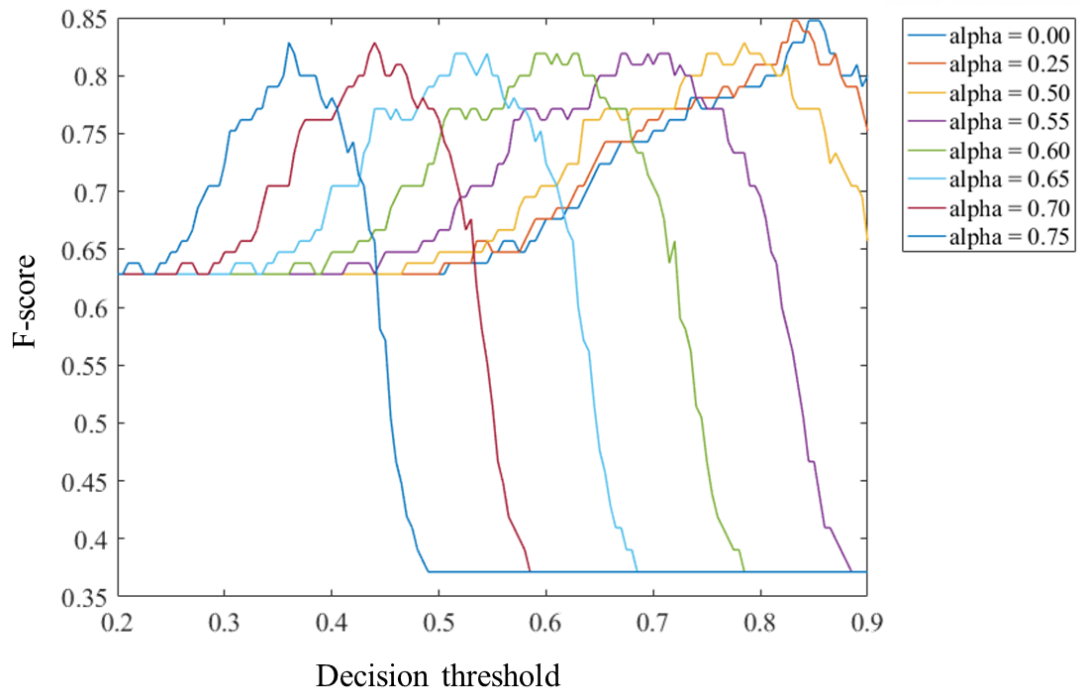


Figure 4-20 The F-scores with respect to the final decision threshold by changing the weight value(α)

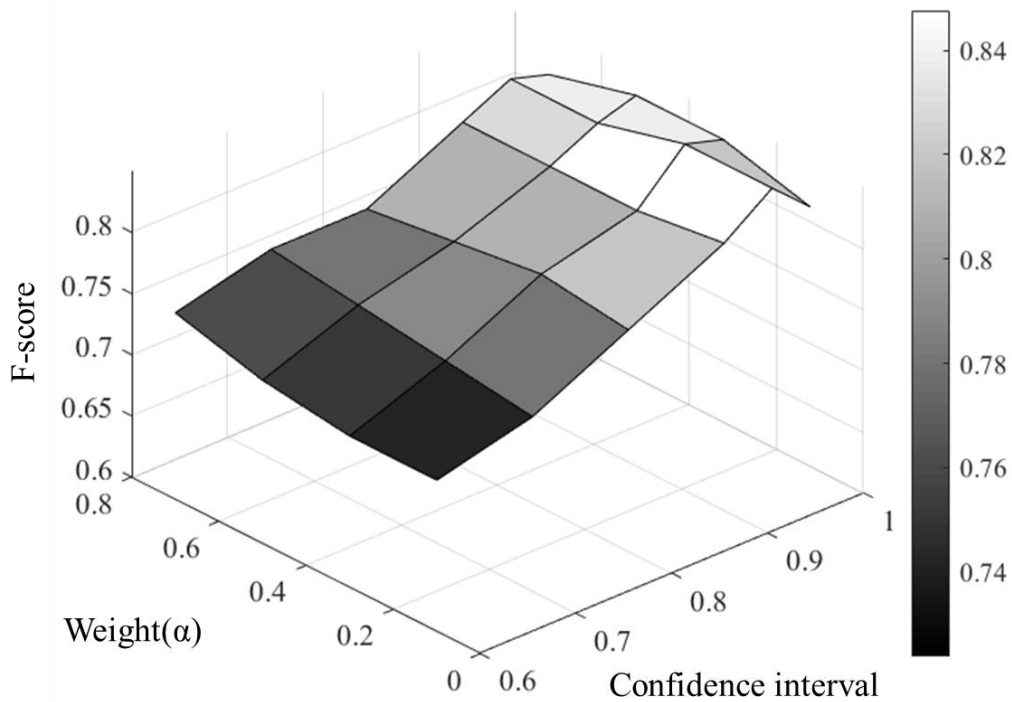


Figure 4-21 The highest F-score with respect to the weights and the confidence intervals

Table 4-11 The highest F-scores of the sensitivity analysis with respect to the weights and the confidence intervals.

F-score	Confidence interval					
	0.6	0.7	0.8	0.9	0.95	0.99
Weight (alpha) 0.7	0.752	0.771	0.771	0.810	0.829	0.819
0.5	0.733	0.762	0.781	0.810	0.829	0.838
0.3	0.724	0.752	0.790	0.810	0.848	0.838
0.1	0.724	0.743	0.781	0.819	0.848	0.819

The experimental result and findings are summarized as below.

- ✓ We observed that the sensor fusion of plasma and temperature signal gave the better accuracy regarding the F-score metric rather than just using individual sensors for defect detection.
- ✓ The fusion with the reflection signal resulted in the worse performance of F-score. The sensor fusion of all three sensors(plasma, temperature, and reflection) also decreased compared to the F-score of sensor fusion of temperature and plasma signal.
 - The reflection signal tended to be closely related to the temperature of the laser source. The temperature of laser source itself increased from 20° to 25°. In this manner, the mean value of the reflected laser signal gradually increased.
 - The reflection signal was related to the focal position of the laser beam. The baseline of the reflected signal was different depending on the target stitches.
- ✓ A sensitivity analysis was conducted by changing the weight value(α).
 - The weight(α) has no statistically significant effect on the highest F-score under the condition of fixed confidence interval(0.95).
 - As the weigh(α) decreased, the decision threshold range for ensuring the F-score larger than 0.8 was expanded. It means that the sensitivity of selecting the decision threshold was lessened by decreasing the weight(α).
- ✓ Further, the response surface of the highest F-score with respect to the weight and confidence interval was constructed.
 - The F-score increased as the confidence interval was increased from 0.6 up to 0.95.
 - In the case of the confidence interval of 0.6 and 0.7, the F-score increased as the weight was increased to 0.7.
 - The higher weight implies that we used the original probability distribution information more. Thus, we are able to use the larger confidence interval for more harsher detection.

This Page Intentionally Left Blank

V.LaserWel: A Defect Detection and Monitoring System for Laser Welding

A framework for the LaserWel system, which is a defect detection and monitoring system for laser welding, mainly consists of two phases. The first is an off-line RLW process analysis phase. It is the off-line process analysis step which is catered for defect thresholds for each sensor and the defect pattern guideline by analyzing pre-experimental result and the signal database. The latter is on-line process monitoring phase to detect the weld defects and the size of the part-to-part gap by matching the current monitored signal with the off-line analysis result.

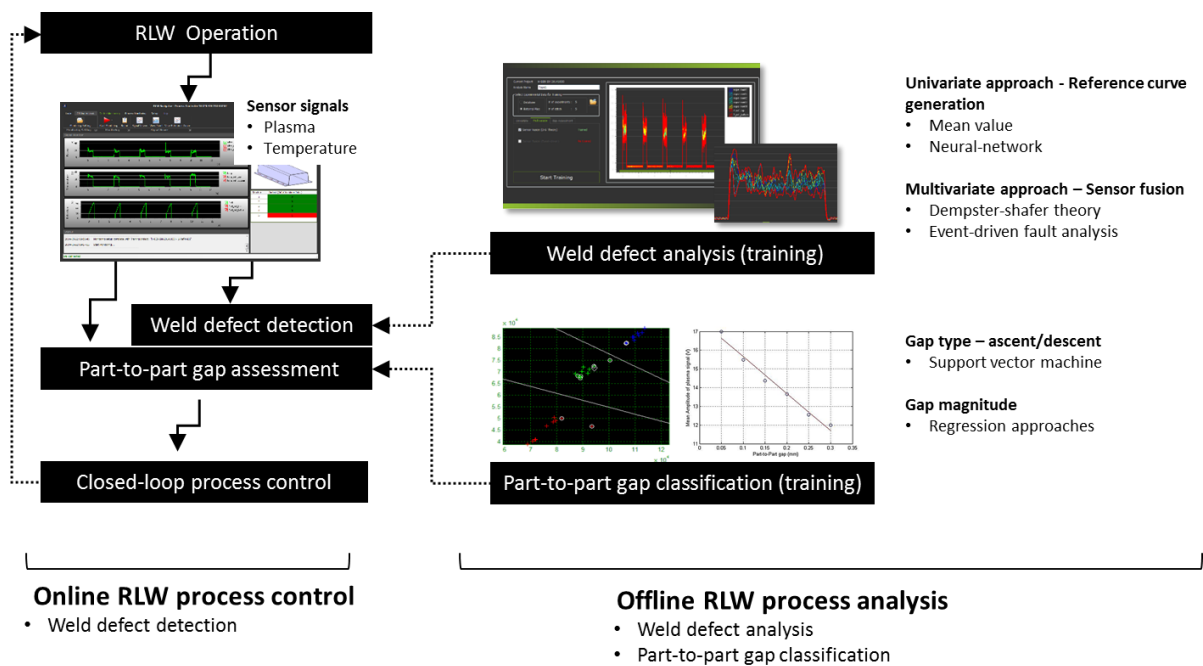


Figure 5-1 A framework for the defect detection and process monitoring system

Off-line process analysis module deals with sufficient pre-experimental data to build models based on the good weld signals. Univariate methods are based on generating the statistical thresholds of each sensor signal, while multivariate methods focus on building good weld pattern using multiple sensor

data simultaneously. Also, part-to-part gap assessment can be done by the current process parameter and corresponding process signals.

In the case of the on-line process monitoring module, online process signal gathered from radiation emission sensors, which are IR range and UV range photodiodes, are analyzed and compared with existing threshold(reference curves) or good weld patterns according to the end-user selection. Also, current part-to-part gap status can be estimated by the trained regression model. Each probability of defect occurrence of the current welding process, and then, will be combined or integrated as one defect measure by using information(sensor) fusion method such as Dempster’s rule of combination.

5.1 Optical system

Laser source

The system consists of a 2.5 axis gantry-based automated welding system with a laser beam from IPG YLS-2000 fiber laser as a laser source. The laser has a maximum output discharge of 2 kW in the TEM01 mode of laser radiation. Table 5-1 lists the technical parameter of the laser source.

Table 5-1 Technical parameters of the laser source (IPG YLS-2000)

Parameters	Unit	Fiber laser
		YLS-2000
Max. laser power	kW	2.0
Beam quality	mm*mrad	6.0
Fiber diameter	μm	600
Emission wavelength	nm	1070
Focal length	mm	278

Data acquisition module

National instrument Compact DAQ(data acquisition module) 9215 with four channels of BNC connectors was selected to gather the electrical signals from the each of sensors. Each channel separately sampled the signal from multiple inputs.

Table 5-2 Technical parameters of the data acquisition system (NI cDAQ 9215)

Parameters	Unit	NI cDAQ 9215
Signal level	V	± 10
Number of channels		4 Differential
Sample rate	kS/s/ch	100
Simultaneous sampling	Y/N	Yes
Resolution	bit	16

Optical sensor module

The sensors system was installed at the side of the laser source. The light signal is gathered along the laser source which is called co-axial acquisition system. We, first, had composed the prototype of the sensor system using the products of Hamamatsu optics.

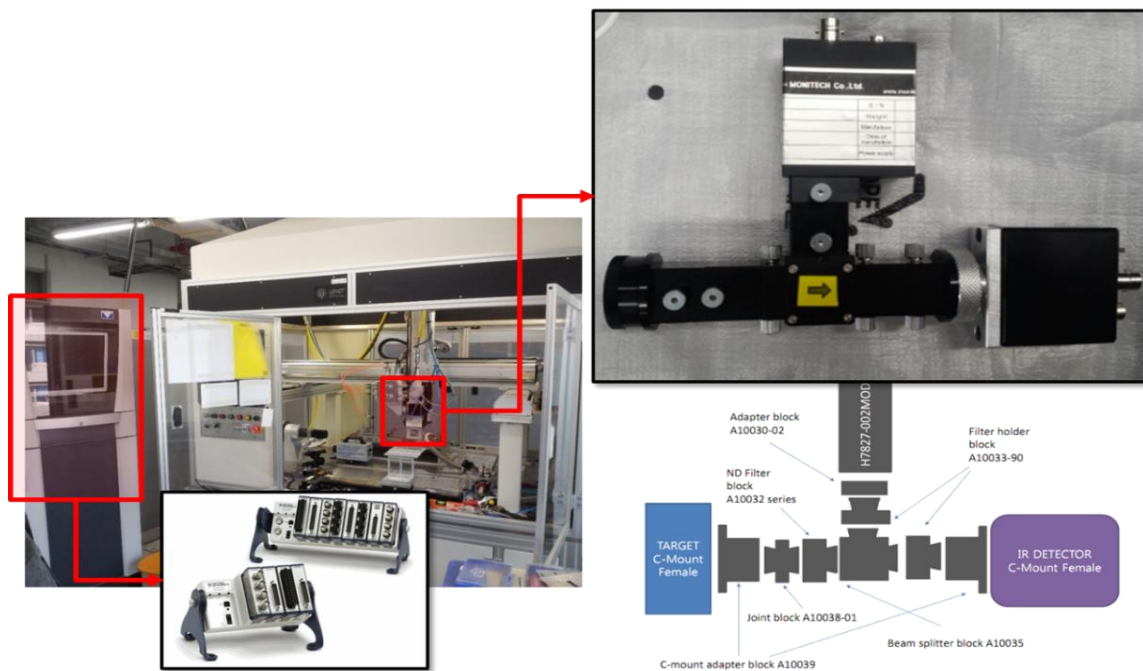


Figure 5-2 A prototype of the sensor system using Hamamatsu optics products

Based on the first prototype, we have configured the improved version of sensor system by utilizing the Thorlab's products. The schematic design of the sensor system and the 3D assembly design is illustrated in Figure 5-3 and Figure 5-4.

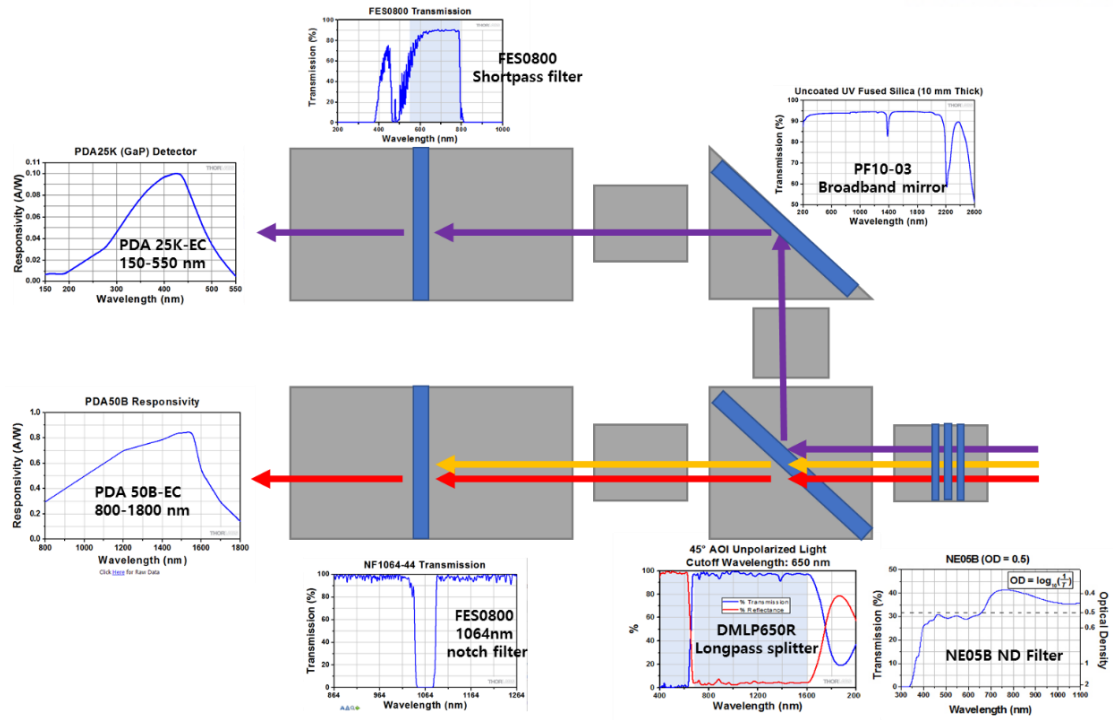


Figure 5-3 The schematic design of the photodiode sensor system for the process monitoring of laser welding

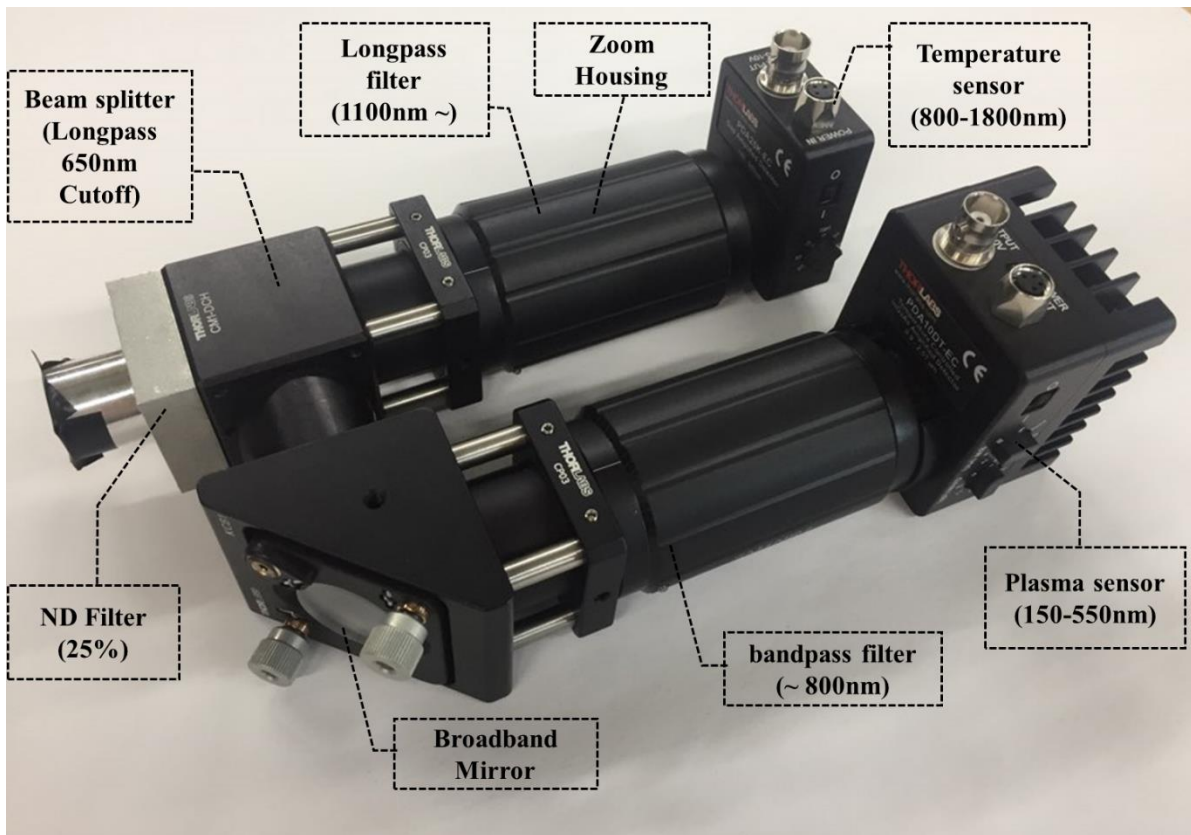


Figure 5-4 3D assembly design for the photodiode sensor system

The data acquisition steps are processed as follows:

- (1) The light signal passes through the neutral distribution filters which can regulate the intensity of the input light source appropriately. The intensity of the input light source decreased to 25% of original one to avoid the clipping effects.
- (2) The light signal is divided into UV range(lower than 650nm wavelengths) and IR range(larger than 650nm wavelengths) by the unpolarized beam splitter. The IR range including the reflected laser beam can pass through the mirror, whereas the light of UV ranges reflected the angle of 45 degrees.
- (3) The splitted light of IR ranges includes the reflected laser beam. The reflected laser beam(1064nm) which is the same as the wavelength of fiber laser source should be removed to get accurate information on weld pool temperature and fluctuation. To do so, we installed the longpass filter of 1100nm which can block the wavelengths of back reflected laser(1064nm) in front of the IR photodiode sensor.
- (4) The split UV range also is filtered by a shortpass filter of 800nm to get rid of unnecessary ranges and assure the UV range information.
- (5) Each of filtered light intensity is converted to the electrical signal which is a range of $\pm 10V$ by the photodiode sensors. We selected Thorlab's photodiode sensors (PDA 25K and PDA 50B) because of reliability and scalability in term of customization.

The detailed specification of the sensor system is in Table 5-3 and Table 5-4.

Table 5-3 Detailed specifications of photodiode sensors



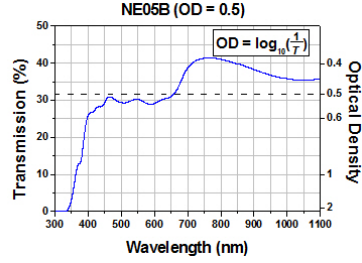
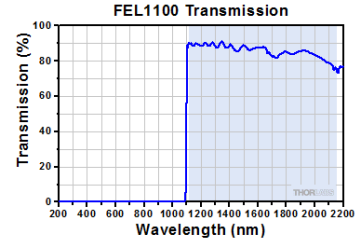
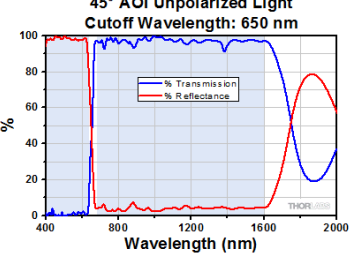
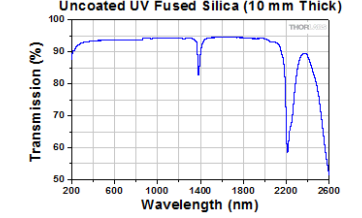
Sensors	Wavelength range (nm)	Detector element	Image
Plasma sensor (Amplified GaP Photodetectors: UV - VIS Wavelengths)	150-550	GaP	
Temperature sensor (Amplified Ge Photodetectors: NIR Wavelengths)	800 - 1800	Ge	

Table 5-4 Detailed specifications of filters for the sensors system

Optical parts	Transmission band (nm)	Cutoff wavelength (nm)	Graph
ND filter	350-2700	350	
Longpass filter (for temperature sensor)	1100-2200	1100	
Beam splitter	685 - 1600	650	
Broadband mirror	200-2200	2600	

5.2 Software development

An overview of the developed software is as follows. The main window can provide information on the sensor signal gathered from the data acquisition system as well as previous experimental data from the database. The current settings such as workspace, reference curves used to detect defects, and selected defect detection methods are easily chosen by the end-user preferences.

Each stitch is analyzed by selected detection method. Defect detection result, and then, are listed in the right bottom table with the different background color of cells(good weld: green, bad weld: red). The specific defect detection information on each stitch are shown when the user double clicked the specific cell in the table.

As the software is connected to the main database, the end-user should log on the database using “Login” menu. Basically, all the data is managed by creating a “Project workspace”. The project, first, should include the production(experiment) date, part specification.

Using the previous experimental data, one can conduct the off-line analysis. The previous data can be loaded from either database or external CSV files. The signal loaded is visualized on the graph window. The signal automatically classifies each stitch. Based on the condition, the off-line analysis method is selected among the reference curve(univariate) generation, defect features, or pattern model(multivariate) generation. Trained reference curves are overlapped and visualized on the right graph window(see Figure 5-6). All the training information and the results belong to the current project workspace. The project can have several off-line training results.



Figure 5-5 A main panel of the developed monitoring software

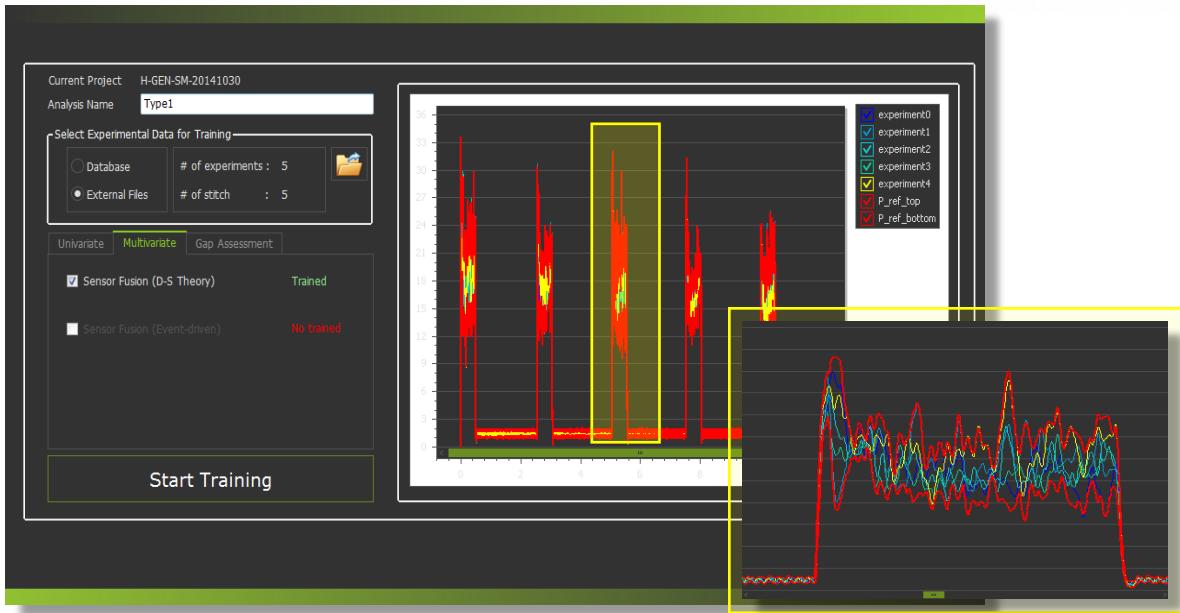


Figure 5-6 An off-line training panel of the developed monitoring software

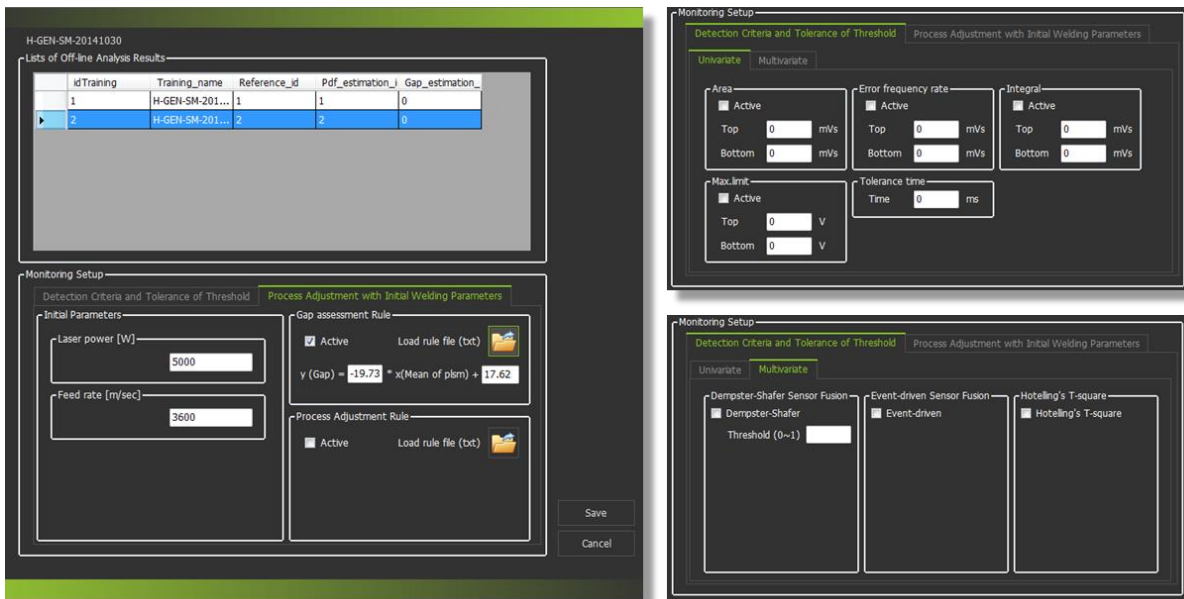


Figure 5-7 A reference selection panel for on-line monitoring of the developed monitoring software

Before the on-line monitoring, an end-user can select one of the previous trained off-line analysis results. Weld defect method is selected based on which off-line analysis is used for training. If training conducted both univariate reference curve generation or thresholds, one could select either of them as a defect detection method. Initial welding parameters such as laser power and welding speed(feed rate) are used for further gap assessment detection criteria.



Figure 5-8 Another version of developed monitoring software for production environment

A compact version of the module is sometimes needed in the case of the production system, even though the developed software is well-functioned and user-centric. For the production environment, we developed another version of the software which is called LaserWel as shown in Figure 5-8.

The main function of this software is focusing on the monitoring the current welding process and defect detection only. Off-line analysis function, database and project management function are removed for compactness and easiness as an aspect of field workers.

The project and trained off-line analysis results from the main software above can be selected by the production software(LaserWel) handler, the total number of the weld, the detected defects, and its specific logs are provided.

This Page Intentionally Left Blank

VI. Conclusion and Future Research

As the use of laser welding application increases so does the needs for reliable quality monitoring methods. For this purpose, attention should be focused on defect detection on the quality estimation of laser welding. Many systems have used statistical approaches for fault detection. There were still limitations in applicability on signals which had a trend. The Dempster-Shafer theory based defect detection method can be advantageously used to overcome the limitations in laser welding process monitoring.

The weld pool temperature, plasma intensity, and back reflected laser signal were gathered regarding the different radiation wavelengths. Their characteristics of nominal trends are estimated by probability distribution function estimation to extract thresholds. We proposed a modified probability assignment function with respect to the thresholds. The weld defect detection of each information source(sensors) was processed respectively. We then aggregated the individual evidence of normal state were fused by using the combination rule of the Dempster-Shafer theory. The performance of the developed detection method is evaluated by statistical comparison of visual inspection result(real defect) and detection result. The result implies that the fusion of the reliable sensors increased the accuracy of defect detection. The defect detection method was eventually embedded in the monitoring software system.

In this thesis, we developed a process monitoring system for laser welding including (i) a hardware configuration of the data acquisition system, (ii) a sensor fusion-based defect detection algorithm for laser welding, and (iii) an easy-to-use GUI-based software that is an essential feature for industrial usage.

We defined the problem or challenging issues on the defect detection of the multi-sensory system.

First, the final decision or classification of the target state cannot be simply achieved by the multiple sensor based monitoring system. It is possible that the individual sensors indicated different decisions in the same state. We adopted the combination rule of the Dempster-Shafer theory as a sensor fuser of the individual defect decisions.

Second, even if all the sensor signals were within the tolerance ranges, the actual defect may have happened in a practical environment. This is an in-tolerance failure problem. We proposed a modified

probability assignment function to adopt the in-tolerance defects. By controlling the slope of the probability assignment function, we were able to treat and assign the uncertainty to the in-tolerance signal at some degree of defect evidence.

The last problem that we did not focus on this thesis was the specific pattern of defect signal that might exist. In this case, we need to model the time-series signal pattern or to choose the number of pieces of segments(called as a binning problem). We also need methods to codify the segmented pieces called a codification problem and to interpret the series of codified segments which is related to the process mining problem.

We further extended the defect detection and monitoring process to the process adjustment. It is a concept of a self-resilient control system which can control the quality automatically. The system appropriately adjusts the laser welding process parameters such as laser power, welding speed, welding direction, in order to recover the current laser welding process from the faulty state. Naturally, statistical analysis of welding experiments must be made a priori in a view to constructing a response surface that proposes appropriate adjust strategies including (i) identification of laser welding process parameters to be adjusted, and (ii) their optimal adjustment magnitudes with respect to the identified welding conditions, especially part-to-part gap. To do this, we will develop a part-to-part gap assessment method to determine the in-process welding condition in a real-time manner. The pilot experiments for the gap assessment model was listed in Appendix. Several regression and classification algorithms such as a support vector machine and neural network will be extended to weld signal trend clustering. By using the results of the part-to-part gap assessment and the associated adjustment strategies, it is possible to expect a better welding quality for the next batches at the same weld part batch of the assembly operation.

Finally, the defect detection module for laser welding, the constructed response surface, and the online part-to-part gap assessment module will be integrated as a closed-loop laser welding process controller. Validation and verification of the developed modules and methods will be carried out.

References

1. R. Oh, D. -Y. Kim, and D. Ceglarek, "The effects of laser welding direction on joint quality for non-uniform part-to-part gaps," *Metals*, vol. 6, no. 8, p. 184, 2016.
2. K. Benyounis and A. Olabi, "Optimization of different welding processes using statistical and numerical approaches—A reference guide," *Advances in Engineering Software*, vol. 39, no. 6, pp. 483-496, 2008.
3. K. Benyounis, A. Olabi, and M. Hashmi, "Effect of laser welding parameters on the heat input and weld-bead profile," *Journal of Materials Processing Technology*, vol. 164, pp. 978-985, 2005.
4. J. Shao and Y. Yan, "Review of techniques for on-line monitoring and inspection of laser welding," *Journal of Physics: Conference series*, vol. 15, no. 1, p. 101, 2005.
5. H. Gu and W. Duley, "A statistical approach to acoustic monitoring of laser welding," *Journal of Physics D: Applied Physics*, vol. 29, no. 3, p. 556, 1996.
6. H. Zeng, Z. Zhou, Y. Chen, H. Luo, and L. Hu, "Wavelet analysis of acoustic emission signals and quality control in laser welding," *Journal of Laser Applications*, vol. 13, no. 4, pp. 167-173, 2001.
7. L. Li, "A comparative study of ultrasound emission characteristics in laser processing," *Applied Surface Science*, vol. 186, no. 1, pp. 604-610, 2002.
8. Y.-W. Park, "Weld process monitoring technology in laser welding," *Journal of Welding and Joining*, vol. 30, no. 1, pp. 27-32, 2012.
9. R. Olsson, I. Eriksson, J. Powell, A. Langtry, and A. Kaplan, "Challenges to the interpretation of the electromagnetic feedback from laser welding," *Optics and Lasers in Engineering*, vol. 49, no. 2, pp. 188-194, 2011.
10. I. Eriksson, J. Powell, and A. Kaplan, "Signal overlap in the monitoring of laser welding," *Measurement Science and Technology*, vol. 21, no. 10, p. 105705, 2010.
11. Y. W. Park, H. Park, S. Rhee, and M. Kang, "Real time estimation of CO₂ laser weld quality for automotive industry," *Optics & Laser Technology*, vol. 34, no. 2, pp. 135-142, 2002.
12. T. Sibillano, A. Ancona, V. Berardi, and P. Lugara, "Correlation analysis in laser welding plasma," *Optics Communications*, vol. 251, no. 1, pp. 139-148, 2005.
13. J. F. Tu, T. Inoue, and I. Miyamoto, "Quantitative characterization of keyhole absorption mechanisms in 20 kW-class CO₂ laser welding processes," *Journal of Physics D: Applied Physics*, vol. 36, no. 2, p. 192, 2002.
14. Y. Zhang, L. Li, and G. Zhang, "Spectroscopic measurements of plasma inside the keyhole in deep penetration laser welding," *Journal of Physics D: Applied Physics*, vol. 38, no. 5, p. 703, 2005.
15. F. Bardin, A. Cobo, J. M. Lopez-Higuera, O. Collin, P. Aubry, T. Dubois, M. Högström, P. Nysten, P. Jonsson, and J. D. Jones, "Optical techniques for real-time penetration monitoring for laser welding," *Applied Optics*, vol. 44, no. 19, pp. 3869-3876, 2005.
16. D. You, X. Gao, and S. Katayama, "Review of laser welding monitoring," *Science and Technology of Welding and Joining*, vol. 19, no. 3, pp. 181-201, 2014.
17. H. Park and S. Rhee, "Analysis of mechanism of plasma and spatter in CO₂ laser welding of galvanized steel," *Optics and Laser Technology*, vol. 31, no. 2, pp. 119-126, 1999.
18. D. Colombo and B. Previtali, "Fiber laser welding of titanium alloys and its monitoring through the optical combiner," *proceedings of International Congress on Applications of Lasers & Electro-Optics*, pp. 620-629, 2009
19. M.-K. Jeon, W.-B. Kim, G.-C. Han, and S.-J. Na, "A study on heat flow and temperature monitoring in the laser brazing of a pin-to-plate joint", *Journal of Materials Processing Technology*, vol. 82, no. 1, pp. 53-60, 1998.
20. C. Kim, J. Kim, H. Lim, and J. Kim, "Investigation of laser remote welding using disc laser", *Journal of Materials Processing Technology*, vol. 201, no. 1, pp. 521-525, 2008.
21. ISO, BSEN. 13919-1: 1997, "Welding-Electron and laser beam welded joints-Guidance on

- quality levels for imperfections-Part 1", 1996.
22. ISO, EN. 13919-2: 2001, "Welding-Electron and laser beam welded joints–Guidance on quality levels for imperfections–Part 2", 2001.
 23. J. Beersiek, "A CMOS camera as a tool for process analysis not only for laser beam welding", *International Congress on Applications of Lasers & Electro-Optics*, 2001.
 24. J. Beersiek, "On-line monitoring of keyhole instabilities during laser beam welding", *International Congress on Applications of Lasers & Electro-Optics*, vol. 99, 1999.
 25. Y. Zhang, R. Kovacevic, and L. Li, "Characterization and real-time measurement of geometrical appearance of the weld pool", *International Journal of Machine Tools and Manufacture*, vol. 36, no. 7, pp. 799-816, 1996.
 26. C. Brock, F. Tenner, F. Klämpfl, R. Hohenstein, and M. Schmidt, "Detection of weld defects by high speed imaging of the vapor plume", *Physics Procedia*, vol. 41, pp. 539-543, 2013.
 27. H. Luo and X. Chen, "Laser visual sensing for seam tracking in robotic arc welding of titanium alloys", *The International Journal of Advanced Manufacturing Technology*, vol. 26, no. 9, pp. 1012-1017, 2005.
 28. W. Huang and R. Kovacevic, "A laser-based vision system for weld quality inspection", *Sensors*, vol. 11, no. 1, pp. 506-521, 2011.
 29. W. Huang and R. Kovacevic, "Development of a real-time laser-based machine vision system to monitor and control welding processes", *The International Journal of Advanced Manufacturing Technology*, vol. 63, no. 1-4, pp. 235-248, 2012.
 30. V. Kaftandjian, O. Dupuis, D. Babot, and Y. M. Zhu, "Uncertainty modelling using Dempster–Shafer theory for improving detection of weld defects", *Pattern Recognition Letters*, vol. 24, no. 1, pp. 547-564, 2003.
 31. N. Nacereddine, M. Zemat, S. Belaifa, and M. Tridi, "Weld defect detection in industrial radiography based digital image processing", *Transactions on Engineering Computing and Technology*, vol. 2, pp. 145-148, 2005.
 32. C.-J. Lee, J.-D. Kim, and Y.-C. Kim, "Study on monitoring of plasma emission signal in lap welding of Zn coated steel sheet using CO₂ laser", *International Journal of Precision Engineering and Manufacturing*, vol. 16, no. 3, pp. 495-500, 2015.
 33. J.-D. Kim and C.-J. Lee, "Study on the Relationship Between Emission Signals and Weld Defect for In-Process Monitoring in CO₂ Laser Welding of Zn-Coated Steel", *Transactions of the Korean Society of Mechanical Engineers A*, vol. 34, no. 10, pp. 1507-1512, 2010.
 34. D. H. Kim, H. J. Shin, and Y. T. Yoo, "A study on the digital filter and wavelet transform of monitoring for laser welding", *Journal of the Korean Society for Precision Engineering*, vol. 30, no. 1, pp. 67-76, 2013.
 35. S. Saludes Rodil, R. Aranz Gómez, J. M. Bernárdez, F. Rodríguez, L. J. Miguel, and J. R. Perán, "Laser welding defects detection in automotive industry based on radiation and spectroscopical measurements", *The International Journal of Advanced Manufacturing Technology*, vol. 49, no. 1, pp. 133-145, 2010.
 36. D. Bebiano and S. C. Alfaro, "A weld defects detection system based on a spectrometer", *Sensors*, vol. 9, no. 4, pp. 2851-2861, 2009.
 37. H. Luo, H. Zeng, L. Hu, X. Hu, and Z. Zhou, "Application of artificial neural network in laser welding defect diagnosis", *Journal of Materials Processing Technology*, vol. 170, no. 1, pp. 403-411, 2005.
 38. I. Eriksson and A. Kaplan, "Evaluation of laser weld monitoring: a case study", *International Congress on Applications of Lasers & Electro-Optics*, vol. 102, pp. 1419-1425, 2009.
 39. D. Colombo, B. M. Colosimo, and B. Previtali, "Comparison of methods for data analysis in the remote monitoring of remote laser welding", *Optics and Lasers in Engineering*, vol. 51, no. 1, pp. 34-46, 2013.
 40. Y. Li, Y. F. Li, Q. L. Wang, D. Xu, and M. Tan, "Measurement and defect detection of the weld bead based on online vision inspection", *IEEE Transactions on Instrumentation and Measurement*, vol. 59, no. 7, pp. 1841-1849, 2010.
 41. P. Zhang, L. Kong, W. Liu, J. Chen, and K. Zhou, "Real-time monitoring of laser welding based on multiple sensors", *Control and Decision Conference*, pp. 1746-1748, 2008.

42. A. Sun, E. Kannatey-Asibu Jr, and M. Gartner, "Monitoring of laser weld penetration using sensor fusion", *Journal of Laser Applications*, vol. 14, no. 2, pp. 114-121, 2002.
43. M. Kuhl and R. Neugebauer, "Quality and process control of Nd: YAG-laser welding using fuzzy pattern recognition techniques for multisensor systems", *IEEE Conference on Emerging Technologies and Factory Automation*, pp. 1329-1332, 2006.
44. O. Basir and X. Yuan, "Engine fault diagnosis based on multi-sensor information fusion using Dempster-Shafer evidence theory", *Information Fusion*, vol. 8, no. 4, pp. 379-386, 2007.
45. J. Ma, F. Kong, W. Liu, B. Carlson, and R. Kovacevic, "Study on the strength and failure modes of laser welded galvanized DP980 steel lap joints", *Journal of Materials Processing Technology*, vol. 214, no. 8, pp. 1696-1709, 2014.
46. W. Chen, P. Ackerson, and P. Molian, "CO₂ laser welding of galvanized steel sheets using vent holes", *Materials & Design*, vol. 30, no. 2, pp. 245-251, 2009.
47. L. Mei, D. Yan, J. Yi, G. Chen, and X. Ge, "Comparative analysis on overlap welding properties of fiber laser and CO₂ laser for body-in-white sheets", *Materials & Design*, vol. 49, pp. 905-912, 2013.
48. L. Mei, G. Chen, X. Jin, Y. Zhang, and Q. Wu, "Research on laser welding of high-strength galvanized automobile steel sheets", *Optics and Lasers in Engineering*, vol. 47, no. 11, pp. 1117-1124, 2009.
49. D. Westerbaan, D. Parkes, S. Nayak, D. Chen, E. Biro, F. Goodwin, and Y. Zhou, "Effects of concavity on tensile and fatigue properties in fibre laser welding of automotive steels", *Science and Technology of Welding and Joining*, vol. 19, no. 1, pp. 60-68, 2014.
50. A. K. Sinha, D. Y. Kim, and D. Ceglarek, "Correlation analysis of the variation of weld seam and tensile strength in laser welding of galvanized steel", *Optics and Lasers in Engineering*, vol. 51, no. 10, pp. 1143-1152, 2013.
51. R. Oh and D. -Y. Kim, "A fault detection method of laser welding based on PDF estimation and Dempster-Shafer theory", *Proceedings of the Society of CAD/CAM Engineers Conference*, 2014, pp. 1011-1016.
52. G. Shafer, "Dempster-Shafer theory", *Encyclopedia of Artificial Intelligence*, pp. 330-331, 1992.
53. K. Sentz and S. Ferson, "Combination of evidence in Dempster-Shafer theory", *Sandia National Labs., Albuquerque, NM (US); Sandia National Labs., Livermore, CA (US)* 2002.
54. P. Smets, "Belief functions: the disjunctive rule of combination and the generalized Bayesian theorem", *International Journal of Approximate Reasoning*, vol. 9, no. 1, pp. 1-35, 1993.
55. Q. Chen and U. Aickelin, "Anomaly detection using the Dempster-Shafer method", SSRN: <http://dx.doi.org/10.2139/ssrn.2831339>, 2006.
56. M. Goldstein and S. Uchida, "A comparative evaluation of unsupervised anomaly detection algorithms for multivariate data", *PloS One*, vol. 11, no. 4, p. e0152173, 2016.
57. C. Siaterlis and B. Maglaris, "Towards multisensor data fusion for DoS detection", *Proceedings of the 2004 ACM symposium on Applied computing*, 2004, pp. 439-446: ACM.
58. G. Shafer, "Dempster's rule of combination", *International Journal of Approximate Reasoning*, vol. 79, pp. 26-40, 2016.
59. G. Shafer, "A mathematical theory of evidence", *Princeton University Press*, 1976.
60. C. Thomas and N. Balakrishnan, "Advanced sensor fusion technique for enhanced intrusion detection", *IEEE International Conference on Intelligence and Security Informatics*, pp. 173-178, 2008.
61. A. Patcha and J.-M. Park, "An overview of anomaly detection techniques: Existing solutions and latest technological trends", *Computer Networks*, vol. 51, no. 12, pp. 3448-3470, 2007.

Acknowledgments

I would like to express my sincere gratitude to my advisor Professor Duck-Young Kim for the continuous support of my study, for his patience, motivation, and immense knowledge. The door of his office was always open whenever I ran into a trouble and had a question about my research or writing. He consistently allowed this paper to be my own work, but steered me in the right the direction. Besides my advisor, I would like to thank the rest of my thesis committee: Prof. Daeil Kwon and Prof. Hyungson Ki for their insightful comments and encouragement, but also for the hard question which incented me to widen my research from various perspectives.

I would like to thank my fellow labmates in for the stimulating discussions, for the sleepless nights we were working together before deadlines, and for all the fun we have had.

Special thanks to going to Sungwoo Hitech Co. Ltd. for supporting the experiments with the 6.6kw disk laser welding system. and also thanks to the financial supports by the international collaborative R&D program of Korea Institute for Advancement in Technology (Grant no. EUFP-M0000224) and the EU FP7 project of the European Commission (Grant no. FP7 Project 285051).

Finally, I must express my very profound gratitude to my family and to my girlfriend for providing me with unfailing support and continuous encouragement throughout for many years. This accomplishment would not have been possible without them.

Thank you.

Appendix

A. Experiments for the part-to-part gap size

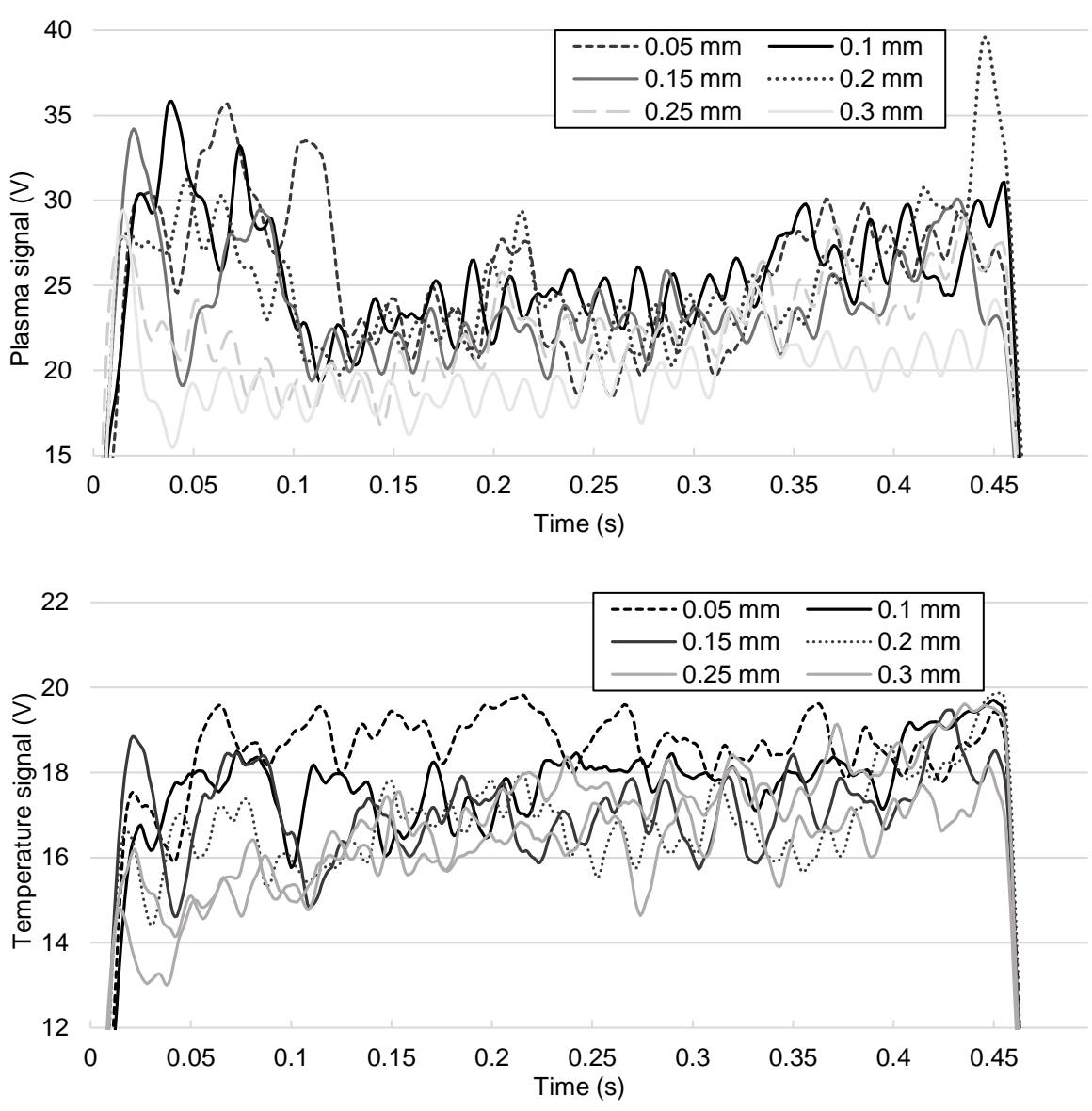


Figure A-1 A trend of the plasma signal and temperature signal on the part-to-part gap size

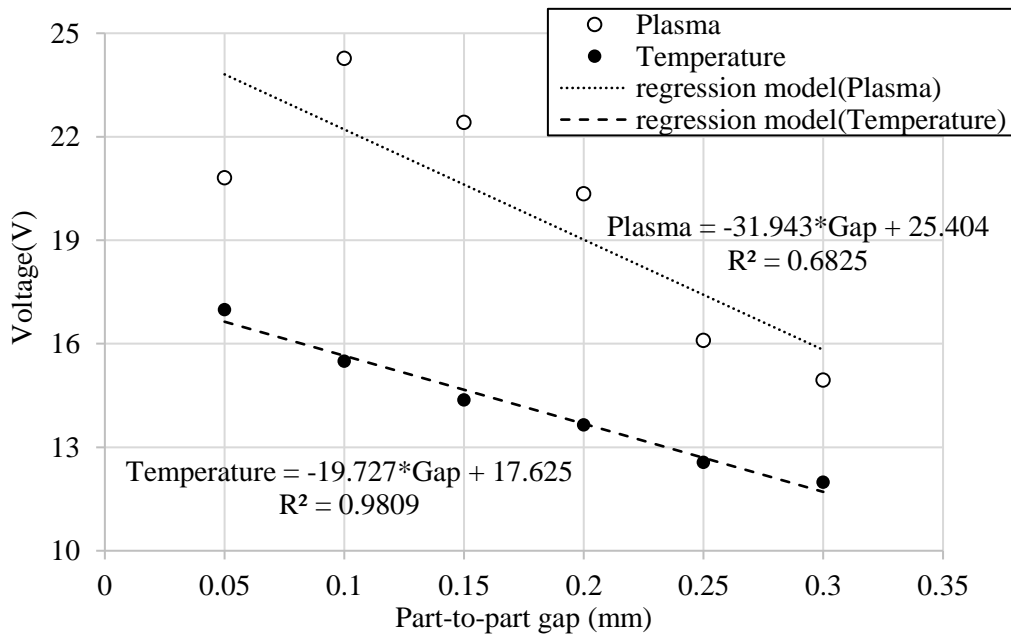


Figure A-2 A simple regression model (light intensity vs. part-to-part gap)

Table A-1 Partial fraction factorial design including center points with three process parameters at two-levels

Code unit	Experimental factors		
	Laser power (W)	Welding speed (mm/min)	Part-to-part gap (mm)
-1	1600	700	0.05
1	2000	1100	0.25

Center point: Laser power = 1800W, Welding speed = 900mm/min, Part-to-part gap = 0.15mm

Table A-2 The experimental data for experiment of part-to-part gap assessment

Experimental factors			Responses		
Laser power (W)	Welding speed (mm/min)	Part-to-part gap (mm)	Plasma (V)	Temperature (V)	Reflection (V)
2000	700	0.05	6.348	6.479	2.266
2000	1100	0.25	3.925	13.258	2.278
1600	1100	0.05	3.520	3.989	1.810
2000	700	0.05	6.648	7.065	2.271
1800	900	0.15	3.809	11.256	2.048
1800	900	0.15	3.591	12.373	2.045
1600	1100	0.05	3.658	4.090	1.807
1600	700	0.25	4.082	10.658	1.810
2000	1100	0.25	4.269	13.572	2.273

2000	700	0.05	6.337	7.531	2.270
1800	900	0.15	3.417	11.119	2.051
1800	900	0.15	3.643	11.597	2.055
1600	700	0.25	3.460	10.798	1.811
2000	1100	0.25	4.985	11.388	2.272
1800	900	0.15	4.552	11.122	2.052
1600	700	0.25	4.697	10.451	1.809
1600	1100	0.05	3.723	4.211	1.808
2000	700	0.05	6.348	6.479	2.266
2000	1100	0.25	3.925	13.258	2.278
1600	1100	0.05	3.520	3.989	1.810
2000	700	0.05	6.648	7.065	2.271

Table A-3 ANOVA table of response surface regression for the experiment of part-to-part gap assessment

Source	Degree of freedom	Sum of squares	Mean square	F-ratio	P-value
Laser power	1	25.047	25.047	80.03	0
Welding speed	1	0.373	0.373	1.19	0.291
Part-to-part gap	1	151.479	151.479	483.98	0
Laser power * Laser power	1	31.107	31.107	99.39	0
Error	16	5.008	0.313		
Total	20	222.419			

R-square = 0.97775

$$Temperature(V) = -236.3 + 0.2646 \times Laser\ power(W) + 31.28 \times Part\text{-to}\text{-part}\ gap(mm) - 0.000072 \times Laser\ power(V) \times Laser\ power(V)$$

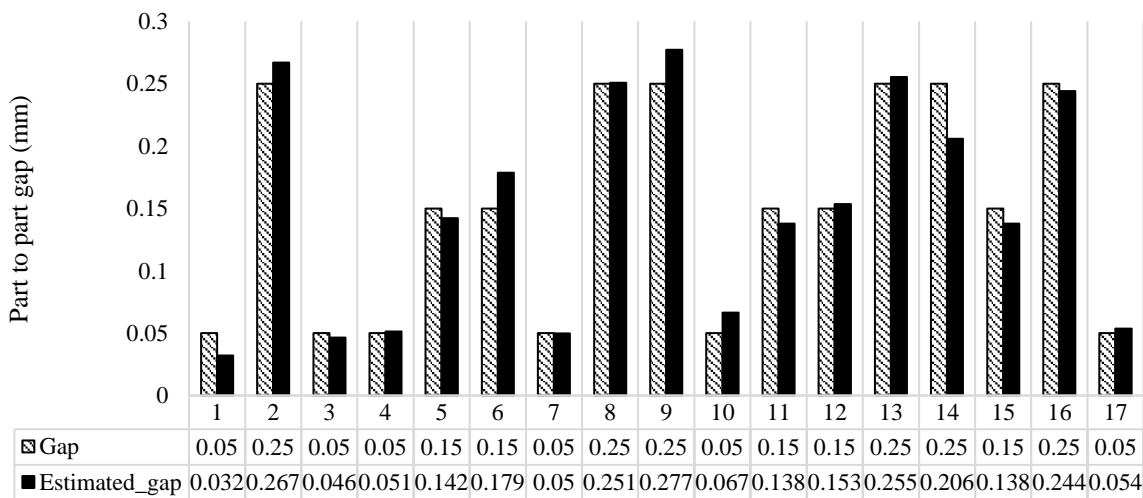


Figure A-3 The estimated part-to-part gap size by the response surface model

B. Software registration

레이저 용접 결함분석 시스템(RLW Navigator Process Controller - Fault Analysis Module)

C-2014-000393-2 (published at 07 / 01 / 2014)

제 C-2014-000393 호	
사	
프로그램 등록증	
1. 프로그램의 제호 (명칭)	레이저 용접 결함분석 시스템(RLW Navigator Process Controller - Fault Analysis Module)
2. 저작자 성명 (법인명)	국립대학법인 울산과학기술대학교 산학협력단 울산 울주군 연양읍
3. 생년월일 (법인등록번호)	230171-0004235
4. 창작연월일	2013년12월01일
5. 공표연월일	2014년01월02일
6. 등록사항	저작자 : 국립대학법인 울산과학기술대학교 산학협력단 창작 : 2013.12.01, 공표 : 2014.01.02
7. 등록연월일	2014년01월07일

「저작권법」 제53조에 따라 위와 같이 등록되었음을 증명합니다.

2014년 01월 10일

한국저작권위원회

